

UC San Diego

UC San Diego Electronic Theses and Dissertations

Title

Ultracompact Computational Spectroscopy and Hyperspectral Imaging

Permalink

<https://escholarship.org/uc/item/6cx2x9jr>

Author

Obheroi, Sonika

Publication Date

2018

Peer reviewed|Thesis/dissertation

UNIVERSITY OF CALIFORNIA SAN DIEGO

Ultracompact Computational Spectroscopy and Hyperspectral Imaging

A thesis submitted in partial satisfaction of the requirements
for the degree Master of Science

in

Electrical Engineering (Photonics)

by

Sonika Obheroi

Committee in charge:

Professor Zhaowei Liu, Chair
Professor Joseph E. Ford
Professor Shayan Mookherjea

2018

Copyright
Sonika Obheroi, 2018
All rights reserved.

The Thesis of Sonika Obheroi is approved, and it is acceptable in quality and form for publication on microfilm and electronically,

Chair

University of California San Diego

2018

Dedication

To my beloved grandpa, for inspiring me to be curious; to envision practical solutions and technological breakthroughs. I'd have loved to share my research topic with you.
I miss you, and your delightful stories!

To my parents, whose constant support and round-the-(international-)clock guidance means the world.

To my younger sister, who, I concede, is the smarter one!
This is for all your cheerful advice, my cherub.

Epigraph

“Measure what can be measured,
and make measurable what cannot be measured.”

Galileo Galilei

Table of Contents

Signatures Page	iii
Dedication Page	iv
Epigraph	v
Table of Contents	vi
List of Figures and Tables	viii
List of Abbreviations	xii
Acknowledgements	xiii
Abstract of the Thesis	xv

CHAPTER ONE

Introduction	1
Background	1
Introduction	3
Proposed Solution	5
Thesis Structure	9

CHAPTER TWO

Measuring with Spectrometers	12
Historical Perspective	12
Working Principle	16
Spectrometer Figures of Merit	21
Trends in Compact Spectrometry	23

CHAPTER THREE

Etalon Array Reconstructive Spectrometry.....	26
Overview.....	26
Operation	32
Outcome	39
Design Analysis	43
Opportunity	59

CHAPTER FOUR

Unconventional Hyperspectral Imaging.....	66
Underlying Principle	66
HS Datacube Acquisition	69
Contemporary Designs.....	71
Unconventional HS Reconstruction using Spectral Resonance Modulation	72
Piezoactuated Etalon.....	73
Elastomeric Etalon	77
One-D Stepped Etalon Array	79
Epilogue.....	83

List of Figures and Tables

<i>Figure 1.1: High performance dispersion spectrometers are inherently big and bulky.....</i>	<i>3</i>
<i>Figure 1.2: A 10 by 10 array of etalons of size 500 by 500 microns for reconstructive spectrometry in the visible wavelength region.....</i>	<i>8</i>
<i>Figure 2.1: Spectrum, first observed by Sir Isaac Newton.....</i>	<i>14</i>
<i>Figure 2.2: Simple prism spectrometer setup for breaking down white light into component wavelengths. This is then incident on a sample and a wavelength dependent light-matter interaction is recorded.....</i>	<i>18</i>
<i>Figure 2.3: Chemical Spectrum of Methane and frequently used scales of measurement.....</i>	<i>19</i>
<i>Table 2.1: Types of Spectroscopy across the electromagnetic spectrum.....</i>	<i>20</i>
<i>Figure 2.4: Schematic diagrams of a. Dispersive Spectrometer, b. Fourier Transform Spectrometer.....</i>	<i>21</i>
<i>Figure 2.5: Spectrometer Figure of Merit: product of resolution and throughput, i.e. ability to distinguish between wavelengths and amount of light that reaches the detector through the system.....</i>	<i>23</i>
<i>Figure 3.1: Planar filter arrays can be integrated directly with sensor array systems for compact spectrometry.....</i>	<i>28</i>
<i>Figure 3.2: Comparison of conventional spectrometric techniques with reconstructive spectrometry (far right). The schematic represents different measurements schemes in which the spectrum is recovered.....</i>	<i>31</i>
<i>Figure 3.3: Etalon Fundamentals. (a) Schematic of a typical optical resonator/etalon, (b) Underlying theory, (c) Transmission spectrum of the etalon for a given optical path length, δ, and reflectivity, R.....</i>	<i>33</i>
<i>Figure 3.4: Impact of cavity thickness on etalon transmission.....</i>	<i>35</i>

<i>Figure 3.5: Sensing Matrix generation by Etalon Array (left) and CS Reconstruction steps (right)</i>	36
<i>Figure 3.6: Spectral Resonance Modulation using Fabry Perot cavities</i>	38
<i>Figure 3.7: Schematic of the Experimental Setup for EARS</i>	39
<i>Figure 3.8: Visualizing the sensing matrix created by the etalon array</i>	40
<i>Figure 3.9: (a) Etalon array illumination using supercontinuum laser with tunable bandpass filters, (b) spectrum reconstruction results, (c) broadband spectrum reconstruction, (d) laser spectrum reconstruction</i>	42
<i>Figure 3.10: Design Parameters in EARS</i>	44
<i>Figure 3.11: EARS Design Procedure</i>	45
<i>Figure 3.12: Nyquist Resolution (Sampling rate) afforded by different cavity thicknesses</i>	47
<i>Table 3.1: Summary of Design Parameters used for the Mid IR Wavelength</i>	48
<i>Figure 3.13: Handbook Formula for Spectrometer Design Parameters</i>	49
<i>Figure 3.14: Better Reconstruction Performance with increasing number of cavities. At lower resolution (25 nm), 30x30 array gives two orders of improvement in reconstruction as compared to 10x10 array for a smaller thickness range</i>	50
<i>Figure 3.15: Better Reconstruction Performance with increasing number of cavities. At higher resolution (7 nm), 30x30 array gives six orders of improvement in reconstruction compared to 10x10 array as the sparsity breaks easily for the given thickness range</i>	50
<i>Figure 3.16: Best Configuration with the 30x30 array. Resolution of 2.5 nm is achieved in the MIR</i>	51
<i>Figure 3.17: Reconstruction Performance with increasing Signal-to-Noise Ratio for an AWGN noise model</i>	52
<i>Figure 3.18: Reconstruction Performance v/s SNR with increasing cavity thickness range from 5 to 50 microns, 5 to 95 microns and 6 to 150 microns. 30 dB is an acceptable SNR limit to CS reconstruction as long as RMSE < 1%, below which signal quality, hence reconstruction, degrades severely</i>	53

<i>Figure 3.18: Hard Thresholding to extract specific spectrum features for reduced number of measurements for recovery.....</i>	<i>54</i>
<i>Figure 3.19: Adaptive Thresholding to extract specific spectrum features for reduced number of measurements for recovery.....</i>	<i>55</i>
<i>Figure 3.20: Increased resolution of 1 nm with a reduced region of interest of 3.2 to 3.4 microns.....</i>	<i>56</i>
<i>Figure 3.21: DWT De-noising.....</i>	<i>58</i>
<i>Figure 3.22: Mathematical Representation of Spectrum Representation in a Sparse Basis. This basis is the chemical spectrum of interest.....</i>	<i>60</i>
<i>Figure 3.23: Accurate Identification of Chemical Sample in a Mixture. RMSE is as low as 0.00026% as there is only one point of measurement.....</i>	<i>61</i>
<i>Table 3.2: Trends with increasing cavity array sizes. Increased number of cavities implies more resolution and reconstruction accuracy.....</i>	<i>62</i>
<i>Table 3.3: Conclusion of design analysis in MIR.....</i>	<i>63</i>
<i>Figure 4.1: Typical hyperspectral dataset measured and hyperspectral line scanner device elements.....</i>	<i>68</i>
<i>Figure 4.2: Mechanisms to acquire the hyperspectral datacube.....</i>	<i>70</i>
<i>Figure 4.3: Recent Advancements in Compact Computational Hyperspectral Imaging.....</i>	<i>71</i>
<i>Figure 4.4: Closed-loop piezoelectric actuation for increasing mirror separation.....</i>	<i>74</i>
<i>Figure 4.5: Schematic for optical setup for HSI with a tunable etalon.....</i>	<i>75</i>
<i>Figure 4.6: Hyperspectral reconstruction with etalon array as test object. A snapshot from the video is shown on the right.....</i>	<i>76</i>
<i>Figure 4.7: Electrostatic pressure causes the elastomer film to shrink when voltage is applied. Calibrating for voltage required per thickness variation.....</i>	<i>77</i>
<i>Figure 4.8: Etalon with elastomer spacer and electrical contacts for actuation.....</i>	<i>78</i>
<i>Figure 4.9: Establishing electrical contacts on the etalon.....</i>	<i>78</i>

Figure 4.10: One Dimensional Stepped Etalon Array with variation only in one direction. Such an array be scanned through the object to encode each pixel of image line-by-line.....80

Figure 4.11: Schematic for optical setup for HSI with a one dimensional etalon array.....81

List of Abbreviations

AOTF	Acousto-Optic Tunable Filter
AWGN	Additive White Gaussian Noise
CCD	Charge Coupled Device
CMOS	Complementary metal-oxide semiconductor
CS	Compressive Sensing
DCT	Discrete Cosine Transform
EARS	Etalon Array Reconstructive Spectroscopy
FTIR	Fourier Transform Infrared Spectroscopy
FP	Fabry Perot
FWHM	Full Width Half Maximum
HS	Hyperspectral
IR	Infrared
l_1 norm	Least Absolute Deviations
LCD	Liquid Crystal Display
LVTF	Linearly Varying Tunable Filter
LWIR	Long Wave Infrared
MIR	Mid Infrared
MMSE	Minimum Mean Square Error
NIR	Near Infrared
RGB	Red Green Blue
RMSE	Root Mean Square Error
SNR	Signal to Noise Ratio
SWIR	Short Wave Infrared
UV	Ultraviolet

Acknowledgements

It has been my utmost honor to be a part of the dynamically inspiring Zhaowei Liu Research Lab. My sincere thanks to Professor Zhaowei for being a motivating mentor and my guiding light; for his invaluable advice, unstinting support and inspirational ideas that strengthened my resolve to research relentlessly and explore extensively.

The learnings as a part of this thesis are an indispensable result of my discussions with Eric Huang, Ph.D. Thank you, Eric, for all the trainings, the creative problem-solving and for being so patient with guiding me through. Your Etalon Arrays are groundbreaking!

I also extend my immense gratitude to all other members of the group: Anna Bezyrdina, Ph.D. for being a constant pillar of support, and for each time you doubled-up as my 'search' option for components in the lab; Qian Ma, Ph.D. and Haoliang Qian for training me in using lab equipment, for always helping me with a smile; Larousse Khosravi, Ph.D. and Yeon Ui Lee, Ph.D. for making me conscious of my entrepreneurial abilities and encouraging me at all times; Jeff Chen, Kaiming Liu and Junxiang Zhao for the fabrication and simulation advice; and to everyone else who made experimenting with Optics even more fascinating.

The members of SPIE, the International Society of Optics and Photonics, has made a world of difference to my confidence as a 'woman in Optics'. Thank you, SPIE, for the multiple distinctions you bestowed on me - the education scholarships, travel scholarships, outreach opportunities; and for giving me the honor of being the Face of Photonics, Dec 2017. Cheers to all the effort that you have put into providing a global platform for Optics enthusiasts that brings the widespread community so much closer.

My special and profound thanks to Prof. Shayan Mookherjea and Prof. Joseph Ford for their precious guidance and encouragement. I am eternally blessed and grateful to have been nurtured by such great minds who have instilled in me the virtue to perennially seek knowledge. It was a true privilege learning from both of you as your Teaching Assistant.

Shout out to the students in my TA classes and labs! Wish you all great success in life!

ABSTRACT OF THE THESIS

Ultracompact Computational Spectroscopy and Hyperspectral Imaging

by

Sonika Obheroi

Master of Science in Electrical Engineering (Photonics)

University of California San Diego, 2018

Professor Zhaowei Liu, Chair

Spectroscopy is a salient practice for the identification and measurement of matter, but typical spectrometers are limited in both scope and efficiency with the current bulky benchtop apparatus. With space exploration becoming rampant, battlefield surveillance critical and forensic investigation real-time, the spectral analysis greatly warrants quick decision making in a compact, portable form factor without sacrificing performance.

Targeting the infrared spectrum, where each substance has its own unique spectral fingerprint, this thesis proposes the design of such a compact, robust, low-cost IR spectrometer using our recently established method of Etalon Array Reconstructive Spectrometry (EARS), which facilitates even faster signal acquisition owing to the neat application of compressive sensing algorithms. In our method, we use an array of optical resonators (etalons) to uniquely encode the transmission spectrum of incident light, which later acts as a known sensing matrix for spectral reconstruction when recorded by a microbolometer array camera sensor. With a geometry that consists of no moving parts, inexpensive fabrication and added robustness of the versatile reconstruction algorithm, we endeavor to drive rapid and high-resolution spectroscopy.

Furthermore, in an effort to overcome the inherent data deluge in hyperspectral imaging, we are encouraged to extend this study to devising handheld hyperspectral imagers with a high-speed, broadband imaging capability resolving thousands of spectral bands. Here, each pixel of the recorded image contains spectral information of the constituent object in the scene. We anticipate that our technology could easily and inexpensively integrate within the camera architectures in existing electronic systems.

Introduction

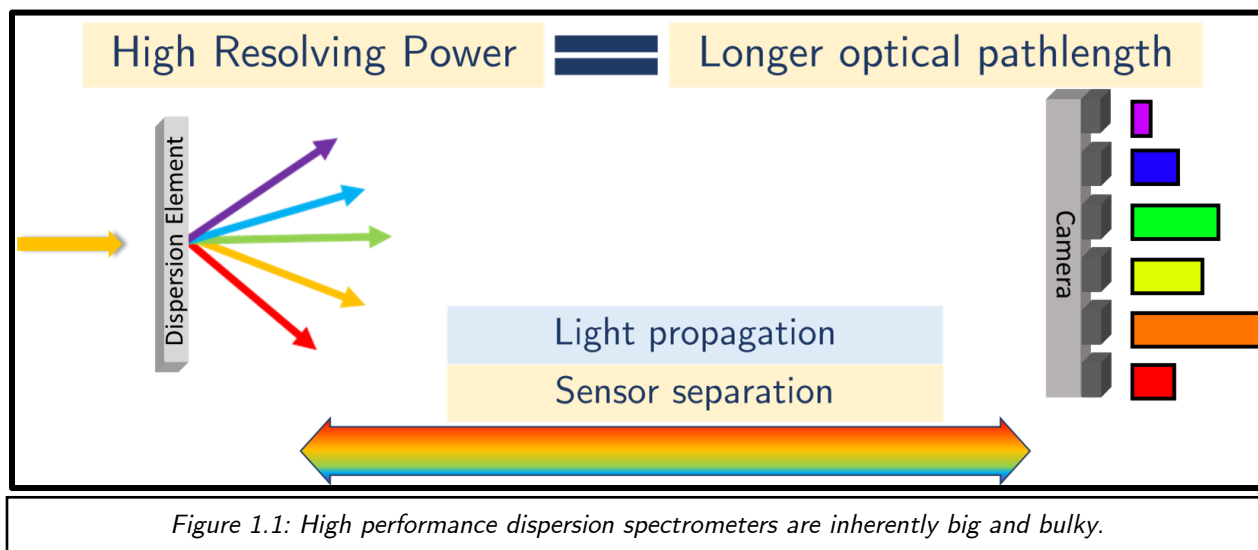
Miniaturizing the Magnum.

1. Background

Spectrometers have long established their significance as the workhorse of much industrial and scientific research. Impacting areas from analytical chemistry to material characterizations, these truly mammoth machines help analyze light-matter interactions by measuring a wavelength-dependent intensity distribution of light which is unique to every substance and thereby aids in identification. Therefore, for the instrument to study light across different wavelengths, it needs a dispersive element that breaks down light into its constituent colors, enough to reveal information about light intensity at distinct wavelengths. One typical figure of merit used to evaluate spectrometers is spectral resolution¹; a figure of how close two measured wavelength components of a spectrum can be while still producing distinct lines resolvable by the spectrometer. Evidently, a higher spectral resolution is desirable. Dating back to Newton's book, 'Opticks'², it became clear that prisms have such a capability, delineated

by the splitting of white light into rainbow colors. They thus emerged as the primary component for spectrometers, albeit at the cost of making the equipment massive, bulky and expensive. Later, diffraction gratings were developed³ that consist of periodic line structures diffracting an incident continuous source of light into different wavelengths and angles. These rapidly became better candidates for spectrometric applications, owing to their relatively compact form factor, ability to disperse light over a wider angle and for their measurement capability in the infrared/UV spectra of light, which are nearly opaque to glass prisms. The problem, again, is that resolving power of these gratings is inversely proportional to the optical path length, which means that the overall spectrometer is still bulky⁴.

Recent advances in fabrication techniques, optical filters, diffractive optical elements, fiber optics, photonic crystals, integrated electronics, detector technologies and data processing algorithms have endeavored to achieve miniaturized spectrometers^{5,6,7,8} with high resolution, broadband detection, higher sensitivity, robust hardware and efficient signal acquisition, but always sacrifice one figure of merit for the other. There is therefore an immense ongoing interest in inventing novel spectrometric devices that can replicate the good performance of traditional spectrometers, even as they are sized down.



2. Motivation

Unlike other fields, Moore's Law has only gradually surfaced in spectroscopy wherein the typical instrument still has an inherently bulky design, limiting the in-filed potential of the science. The key developments are centered either around curating a better wavelength dispersion element, improving the collection optics (e.g. using fibers), or using cheaper, more sensitive sensors for detection. However, the past decade has been particularly encouraging due to the burgeoning breakthroughs in computational algorithmic methods that help overcome the fundamental hardware limitations of both optics and electronics.

One such gigantic research wave is in Compressive Sensing (CS)⁹, which is primarily attractive as it sets out to achieve high resolution by making far fewer measurements than what is theoretically mandated. The CS algorithms suggest that reconstructing an undersampled, sub-Nyquist “compressed” signal is possible, enabling faster acquisitions with lesser data points. The basis of solving the underlying linear inverse problem here is to do with the sparsity of the signal of interest. If the signal is sparse, meaning mostly zero, in any transform domain (Fourier, wavelet, etc.), it is said to be compressible and therefore can be recovered using CS. Here we measure linear projections of the signal in the chosen sparse domain instead of measuring the signal directly. That is, we measure a signal correlated by a sensing waveform, which is essentially known encryption of the analog data. By doing so, the scheme reduces the burden on the hardware architecture surrounding the measurement, albeit at a tiny cost of increased processing complexity. In cases where there are constraints on the physical size, weight and power of the measurement device, the flexible and robust CS solution is extremely suitable.

Since most chemical spectra can be represented sparsely, this thesis seeks out to uniquely use compressive sensing as a tool for computational camera-based spectroscopy¹⁰ by engineering a planar mask-like structure to encode the transmission of light, which would become the known sensing matrix for CS reconstruction. Such a structure could be easily

integrated on top of the camera sensor, using inexpensive fabrication techniques, or inserted in the conjugate image plane of the front imaging optics to produce a compact form factor. The design requirements for such a structure is explored in this study with emphasis on the operation in infrared wavelengths (SWIR: 950 nm – 1250 nm, MWIR: 3 μm – 5 μm and LWIR: 8 μm – 12 μm). In addition, to reduce the actual number of measurements while still retaining performance, CS is appealing to use in hyperspectral image rendering, wherein high spectral resolution otherwise amounts to complex computation and slow acquisition rates. An extended study of the aforementioned structure is conducted for the design and implementation of a hyperspectral imager using compressive sensing reconstruction. Efforts are made to analyze how the practical combination of computational methods can miniaturize spectrometers and hyperspectral imagers, thereby increasing their infield potential.

3. Proposed Solution

To spectrally modulate light in a manner that could represent a known sensing matrix for CS reconstruction¹¹, one solution is to make incident light pass through a structure whose transmission is exactly known. A typical way to achieve this is by generating patterns using spatial light modulators¹², coded aperture patterns¹³, electro-optical liquid crystals¹⁴, digital mirror devices¹⁵ (in reflection mode) or optical resonators¹⁶. Scanning using SLMs or DMDs

are limited to a few MHz, exhibiting mechanical limitations on speed. Additionally, they require a spatial-to-spectral conversion. Optical resonators, however, are like specially designed filters that modulate the spectral resonance uniquely without any speed constraints, reproducing one intensity value per wavelength transmission. An excellent example utilizes traditional Fabry-Perot resonators or etalons (two parallel mirrors facing each other) where the transmission is maximum at resonant wavelengths due to constructive interference, producing a unique transmission spectrum. This spectrum is known, as it depends on chosen parameters of mirror reflectivity (R) and optical path length (δ , refractive index of spacer material and cavity thickness). Therefore, multiple etalons in an array (each with varying parameters) will encode the incident light differently per etalon. The encryption through the entire array is calibrated as the desired sensing pattern. The etalon array is an exceedingly appropriate choice for several reasons: a. 2-D planar structure, with a compact form factor, b. robust mechanical design, c. control over parameters, d. inexpensive fabrication, e. broadband operation. Combined with compressive sensing reconstruction, the same signal is rapidly recovered with far fewer measurements generating a high-resolution spectrum with uncompromised performance, that is not constrained by detector readout speed. This established technique is known as Etalon Array Reconstructive Spectrometry (EARS)¹⁷ and is the primary method delineated in this study. Moreover, the computational working principle inspires the development of an imaging spectrometer (or hyperspectral imager), which unlike traditional imagers, reveals information

in various spectral bands than just the RGB (red, green and blue) colors. Expectedly, such devices have a gigantic amount of data to process for each spectral band (typically 200-400 frames) for high-resolution acquisition. By reducing the number of measurements, CS reconstruction would help reduce processor overload, enabling fast acquisitions.

The objective of this thesis is to identify and implement the design parameters of the etalon array for unconventional reconstructive spectrometry, thus finding a reasonable fit for the hardware and software framework that results in least root mean squared error (RMSE) post processing. An additional purpose of the study is to develop an optical resonator mechanism for a hyperspectral imager such that a similar reconstruction regime can be applied for compact, high-performance and high-resolution hyperspectral image rendering.

The design of the etalon array for computational spectroscopy is aimed towards remote sensing and environmental monitoring applications in the mid-infrared wavelengths between 3 to 5 microns for an industrial collaborator sponsored study. Results for other operational

bandwidths are also included. The hyperspectral imager is discussed for a VIS-SWIR wavelength regime, and a LWIR implementation is introduced.



Figure 1.2: 10 by 10 array of etalons of size 500 by 500 microns for reconstructive spectrometry in the visible wavelength region.

4. Thesis Structure

This study to analyze the design of etalon arrays for reconstructive spectrometry is divided into three chapters. Chapter One, *Measuring with Spectrometers*, offers the requisite background for understanding the working principles and figures of merit of spectrometers. It also briefly introduces the challenge in miniaturization and provides examples of recent advancements in ultracompact spectrometry, with several references for literature review.

Chapter Two, *Etalon Array Reconstructive Spectrometry*, proposes our solution to a miniaturized spectrometer that affords high resolution, fast spectral measurements in a form factor as small as a 5mm × 5mm × 2μm flat optical element that could be integrated directly on top of a camera sensor array. This element is a unique etalon array with varying cavity thicknesses that encode the incident spectrum in a complex albeit well-known manner. The compressive sensing algorithms that make use of this encryption for then reconstructing the actual spectrum are introduced on this chapter. The chief purpose of the study, i.e. elaborating the design requirements of such an element to suit the infrared regime of operation are concisely reported.

Chapter Three, *Unconventional Hyperspectral Imaging*, dovetails into using the concept of complex reconstruction for imaging spectroscopy. Here, each pixel in the image must contain the spectrum of the constituent object and the compressive sensing technique overcomes the

inherent data deluge in existing hyperspectral imagers. Three different configurations to cause the spectral encryption are proposed and potential applications are discussed.

References and Acknowledgements

1. R. G. Bingham, *Grating Spectrometers and Spectrographs Re-examined*, Q. Jl. No 4, Royal Astronomical Society 20, Pg. 395-421 (1979)
2. Newton, I., *Opticks* (Smith & Walford, 1704)
3. E. Loewen and E. Popov, *Diffraction Gratings and Applications* (Marcel Dekker, New York, 1997)
4. Noel H. Wan, Fan Meng, Tim Schröder, Ren-Jye Shiue, Edward H. Chen and Dirk Englund, *High resolution optical spectroscopy using multimode interference in a compact tapered fibre*, Nature Comm. 6, 7762 (2015)
5. Cláudia Santos, Miguel Lopo, Ricardo Páscoa and João Lopes, *A Review on the Applications of Portable Near-Infrared Spectrometers in the Agro-Food Industry*, Applied Spectroscopy Pg. 1215 -1233, Vol 67, No. 11 (2013)
6. J. P. Smith, *Spectrometers get small: Miniature spectrometers rival benchtop instruments*, Anal. Chem. 72:653A–658A (2000).
7. Shao-Wei Wang, Changsheng Xia, Xiaoshuang Chen, Wei Lu, Ming Li, Haiqian Wang, Weibo Zheng and Tao Zhang, *Concept of a high-resolution miniature spectrometer using an integrated filter array*, Opt. Lett. 32, 632–634 (2007)

8. Umpei Kurokawa, Byung Choi and Cheng-chun Chang, *Filter-based miniature spectrometers: spectrum reconstruction using adaptive regularization*, *Sensors Journal*, IEEE 11, 1556–1563 (2011).
 9. Y. C. Eldar and G. Kutyniok, *Compressed Sensing: Theory and Applications* (Cambridge University Press, 2012)
 10. A. Stern, ed., *Optical Compressive Sensing* (CRC Press, 2016).
 11. David J. Starling, Ian Storer, and Gregory A. Howland, "Compressive sensing spectroscopy with a single pixel camera," *Appl. Opt.* 55, 5198-5202 (2016)
 12. A. D. Rodríguez, P. Clemente, E. Irlles, E. Tajahuerce, and J. Lancis, *Resolution analysis in computational imaging with patterned illumination and bucket detection*, *Opt. Lett.* 39, 3888-3891 (2014)
 13. Tsung-Han Tsai and David J. Brady, *Coded aperture snapshot spectral polarization imaging*, *Appl. Opt.* 52, 2153-2161 (2013).
 14. Yitzhak August and Adrian Stern, *Compressive sensing spectrometry based on liquid crystal devices*, *Opt. Lett.* 38, 4996-4999 (2013).
 15. T. Sun and K. Kelly, in *Computational Optical Sensing and Imaging* (Optical Society of America, 2009), pp. TuA5.
 16. Yaniv Oiknine, Isaac August, Dan G. Blumberg, and Adrian Stern, *Compressive sensing resonator spectroscopy*, *Opt. Lett.* 42, 25-28 (2017).
 17. Eric Huang, Qian Ma and Zhaowei Liu, *Etalon Array Reconstructive Spectrometry*, *Scientific Reports* volume 7, Article number: 40693 (2017).
-

Measuring with Spectrometers

Spectrometers measure matter.

1. Historical Perspective

What are spectrometers? How did they first come about? What was their early impact?

Light has utterly fascinating properties that manifest themselves during the intricate ways in which light interacts with matter. Combined with both sample material and medium characteristics that govern the very nature of the interaction, light is appropriately absorbed, scattered, reflected and/or transmitted across different wavelengths, generating a spectrum¹. The spectrometer, also frequently referred to as spectrograph or spectrophotometer in this mode of operation, helps deduce the spectrum of the light thus collected from the sample matter. In other words, it helps understand the light interaction with the sample, which can be used to quantitatively understand the sample. It is a 'spectrum-meter' that measures the

unique spectral information that is contained in this light-matter interaction, often indicating the chemical composition of the matter in question.

From their inception back in the seventeenth century², spectrometers have been invaluable when characterizing and identifying different unknown substances. The momentous moment that established the modern understanding of light and color was when Sir Isaac Newton demonstrated the existence of a light spectrum³. A famous portrait depicts his experiment (see Figure 2.1): he shines sunlight through a narrow slit from his window onto a prism and notices a beautiful rainbow spectrum on a further wall. Later, William Wollaston and Joseph Von Fraunhofer⁴, in 1802 and 1814 respectively, noticed dark lines in the solar spectrum, thereby accidentally founding spectroscopy. It was theorized by Gustav Kirchoff⁵ in 1860 that these dark lines were linked to the absorption of specific wavelengths/frequencies of light by the elements in the sun. His remarkable invention of the diffraction grating based spectrometer is unparalleled and is still used in modern day spectrometers. In 1860, Robert Bunsen and Gustav Kirchoff invented the spectroscope which was the most practical spectroscopic instrument at the time and laid the ground work for recording various chemical spectra.



Figure 2.1: Spectrum, first observed by Sir Isaac Newton. Illustration by Warehouse 13.

The impact of the spectrometer was immense in analytical chemistry⁶, as it helped identify new elements. Rubidium, Cesium, Thallium and Helium were new entrants in the periodic table after being newly identified spectroscopically. Most notable contributions were made in the field of astronomy, where spectroscopy was used to find the elements found in stars, planets, nebulae and galaxies. The detection and identification are crucial for space exploration and earth observations. New technological advancements in optics and electronics made such characterizations far simpler to achieve by not restricting the analysis to the visible bandwidth. When it became possible to detect the “nonvisible photons”, spectroscopy became

possible in the UV and IR regions, thereby making it a standardized procedure for the same by the nineteenth century. In 1940, the first version of a spectrophotometer was introduced by Arnold J. Beckman at National Technological Laboratories, which remains the lab's greatest discovery and was a hit in biological chemistry. From here, many other types of spectrometers were developed from 1950 to 1980, until more reliable, almost automatic instruments took the center stage in spectroscopic applications ranging from medicine to law enforcement.

Note: The purpose of discussing the timeline of spectrometer innovations is to indicate that even though developments in the field were significant in the early years, earning the prestigious Nobel Prize(s)⁷, they were spaced out in time. There has been extensive research in developing high performance miniaturized spectrometers during the past two decades. This surging interest can be largely associated with the recent growth in sophisticated detector technologies, optical systems and integrated electronics, like CCD, CMOS, InGaAs cameras, MEMS devices and silicon photonics. The section on compact computational spectroscopy will explore these inventions (particularly in imaging spectroscopy) in more detail, but it would be helpful if the reader kept a mental note as the pertinent issue chiefly constructs the problem statement for this study.

2. Working Principle

How do spectrometers function? What does the resulting spectral plot look like? What are some traditional types and modes of measurement? Looking inside spectrometers. What are the key components?

We know that spectroscopy represents a detailed analysis of light, or to be specific, electromagnetic radiation, across wavelength by taking advantage of the unique way in which light interacts with matter. Intuitively, the different wavelengths/frequencies of light must be caused to split up and follow different paths before selectively hitting the sample of interest. Then, it can be easily characterized how the sample modifies each incident wavelength (or wavelength range) of light as a sensor integrates the measurement. By detecting how many photons of each energy are transmitted/absorbed from the source to the sensor, an intensity versus wavelength graph is generated, which is also known as the *spectrum*.

A simple spectrometer has the following components⁸:

- *Source*: emitting visible, infrared or ultraviolet electromagnetic radiation. Typical examples are light bulb, halogen lamp, laser, flame, hot ceramic rod, fluorescent tubes, glow lamps, etc.

- *Small slit*: controls the amount of light (photon flux) and angle that enters the spectrometer. It also determines the spectral resolution.
- *Energy Differentiation Unit*: a dispersive component that separates light by frequency, also known as monochromator. This is the central component that makes up the spectrometer and is mainly comprised of a prism (glass, quartz, silicon or salt), diffraction grating (reflective or transmissive, glass or metal or holographic) or optical filters (sensitive narrow band filters, like Fabry-Perot cavity or a similar interferometric setup, filter wheels or multiple integrated filters on top of a sensor array).
- *Sample*: that mainly absorbs or emits light. Certain wavelengths are absorbed by the sample which results in a “peak” in the spectrum (even though intensity passed to the detector is zero here, it is colloquially referred to as peak). The sample can also emit light, like in the case of fluorescence, phosphorescence and Raman scattering.
- *Detector*: integrates the measurement. Refer to figure 2.2 for a pictorial understanding of the key components.

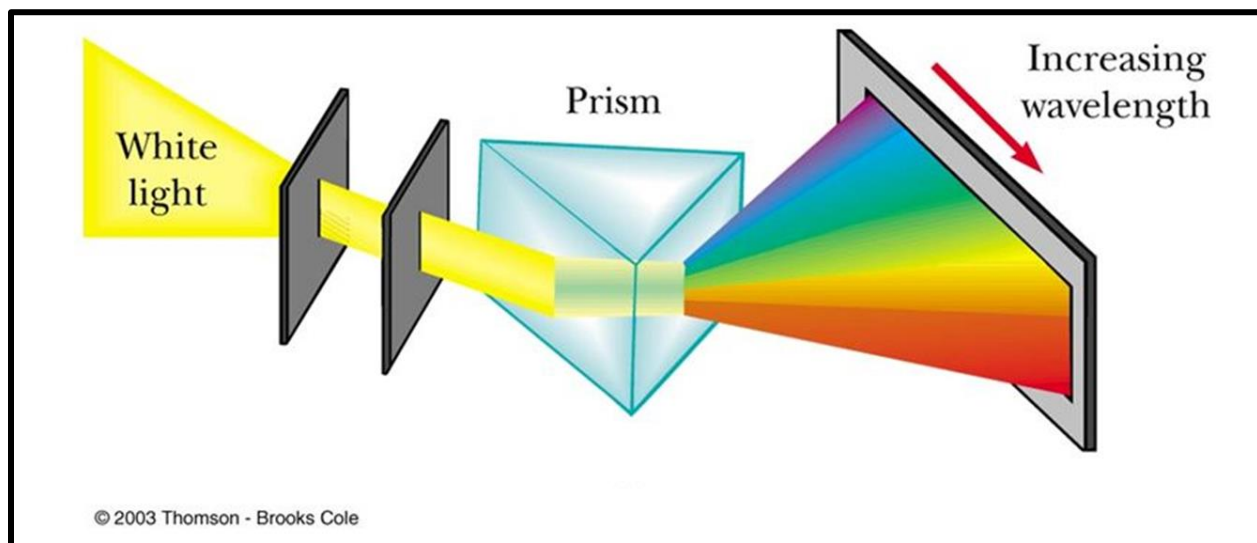


Figure 2.2: Simple prism spectrometer setup for breaking down white light into component wavelengths. This is then incident on a sample and a wavelength dependent light-matter interaction is recorded.

The spectrum formed is a measure of relative intensity of light that reaches the detector with and without the sample. The following figure 2.3 specifies the typical scale for measurement¹. While there are innumerable methods established to record a spectrum, each catering to specific applications, two main classes of spectrometers exist: the dispersive spectrometer⁴, and the Fourier transform spectrometer¹⁰. Figure 2.4 looks inside each of these to provide an understanding of the different spectrum generation methods. This distinction is important to make as this thesis later refers to designing a more powerful, compact spectrometer than the Fourier transform version in the infrared. It is also important to note here that when extending to the non-visible portions of the electromagnetic spectrum, the

optical elements used for spectroscopy must be transparent to the concerned wavelengths⁹.

For example, molecular compounds are not used for optics like lenses, substrates, filters, etc.,

in IR spectrometry as they have their own characteristic vibrational absorptions in this range.

Simple ionic compounds like NaCl, KBr, CaF₂, ZnSe or CsI are used as they are transparent

to infrared light. Therefore, choosing the right materials for spectroscopy must be borne in

mind while designing the spectrometer.

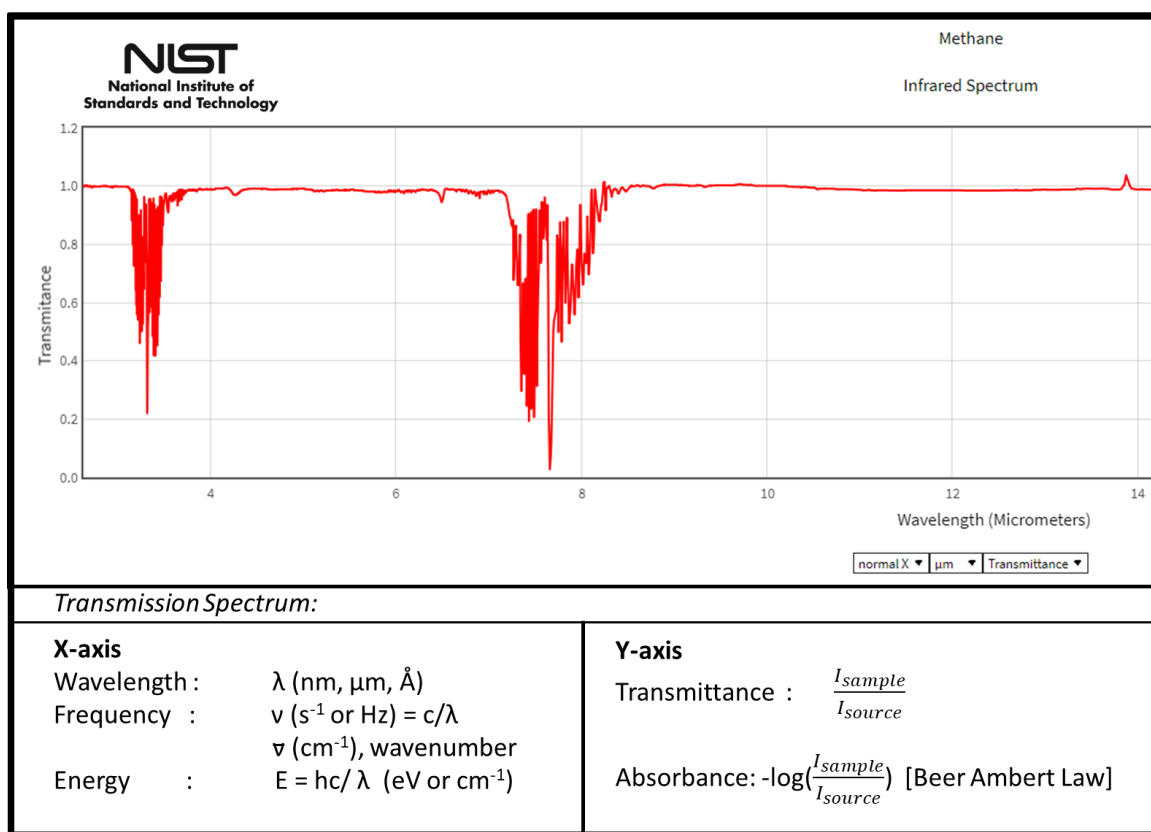


Figure 2.3: Chemical Spectrum of Methane and frequently used scales of measurement.

Table 2.1: Types of Spectroscopy across the electromagnetic spectrum⁸

Region	Spectroscopy	Process Involved
Radio Waves	Nuclear Magnetic Resonance	Changing nuclear spin orientation
Microwave	Electron Spin Resonance	Changing electron spin orientation
	(pure) Rotational	Changing molecular vibrational states
Infrared	Vibrational	Changing molecular vibrational states
Ultraviolet	Electronic	Changing atomic or molecular electronic states
X Ray	Inner electronic	Changing electronic states or ejecting electrons
Gamma Ray	Mössbauer	Changing nuclear energy levels

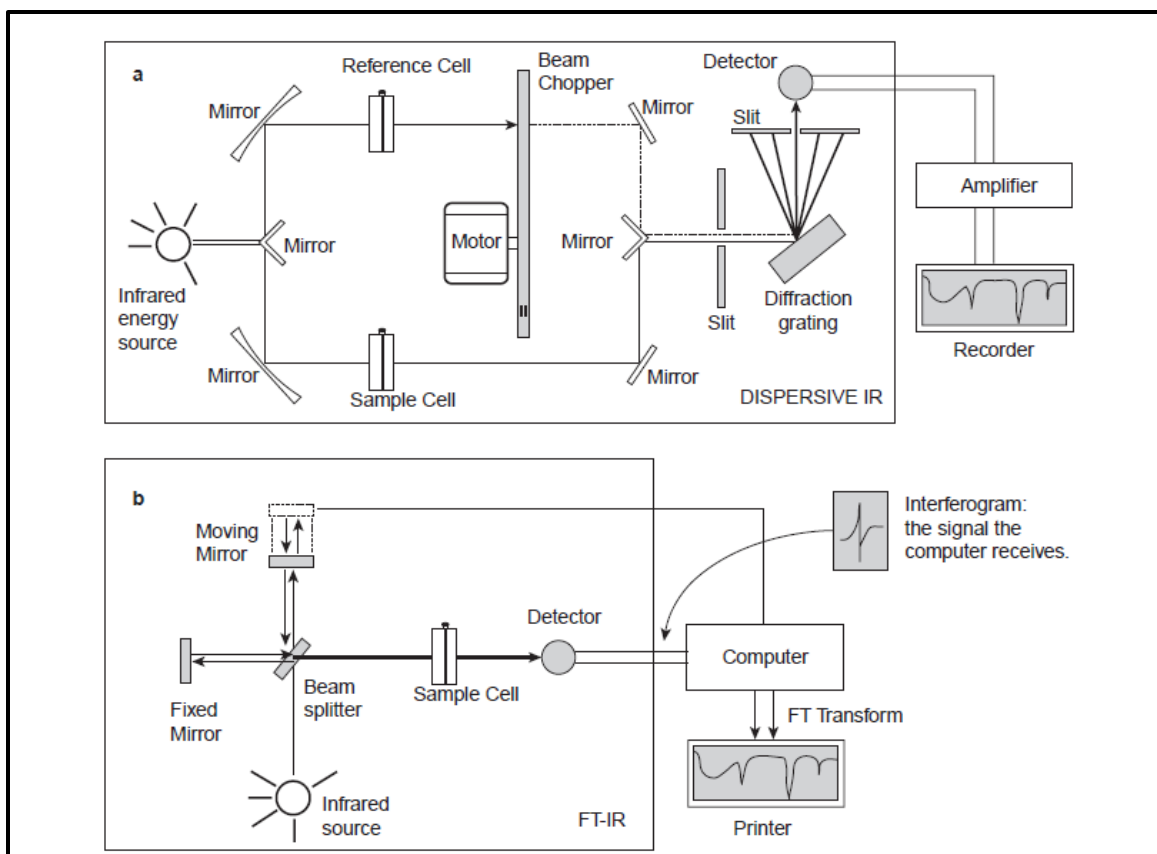


Figure 2.4: Schematic diagrams of a. Dispersive Spectrometer, b. Fourier Transform Spectrometer¹¹

3. Spectrometer Figures of Merit

The figure of merit of a given spectrometer indicates the ability and rate at which that instrument acquires spectral information and can be used to compare alternative designs. Two critical factors that make up the figure of merit are the throughput and resolving power¹². These were first reported by French physicist Pierre Jacquinot¹³. Resolving power is a measure of spectral detail recorded in the spectrum, often given by the wavelength

resolution which is the smallest separation, $\delta\lambda$, of two 'monochromatic' spectral lines that can just be resolved as two by a given spectrograph¹⁴. The dimensionless quantity is given by $\lambda/\delta\lambda$. Even with an infinitesimally narrow slit, Lord Rayleigh in 1879 showed that diffraction effects in the dispersing element inevitably result in finite wavelength resolution, given by diffraction. This depends directly on the aperture A and angular separation $d\theta/d\lambda$, which implies larger elements have higher resolving power¹². For a prism, this leads to higher absorptive loss as angular dispersion and thus, resolving power are greatest at the grazing angle. This also makes alignment challenging. For gratings, resolving power is higher for greater number of lines. Greater propagation is necessary to obtain higher resolution, as resolving power inversely relates with optical pathlength as shown in Fig 1.2. Various design equations are given in Reference 12.

The throughput in practice always wavelength dependent as in Figure 2.5. It can be defined as the fraction of the source photons in the focal plane of the dispersive elements that are recorded by the detector, surviving through unwanted reflection, absorption, scattering or vignetting. Therefore, throughput is a measure of spectrograph efficiency in not losing the light it receives.

The wavelength coverage on single exposure is also a necessary figure of merit however it is highly dependent on the detector sensitivity at different wavelength ranges.

Also, materials used for dispersion, e.g. prisms, have non-linear dispersion loss at certain wavelengths. These must be identified and calculated before the spectrometer design.

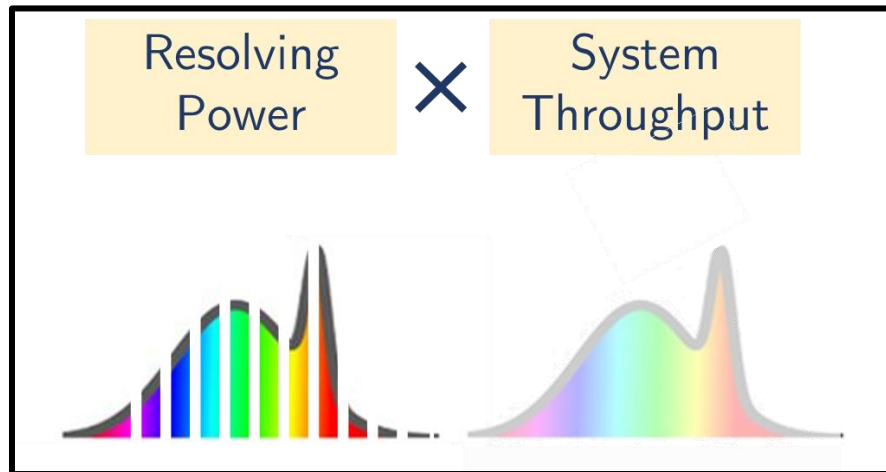


Figure 2.5: Spectrometer Figure of Merit: product of resolution and throughput, i.e. ability to distinguish between wavelengths and amount of light that reaches the detector through the system.

4. Trends in Compact Spectroscopy

The invention of filter-based spectrometers was a step closer to compact spectrometry. Here, multiple narrowband filters are integrated on top of each pixel in camera array detectors like the CCD. Each filter transmits the component of light around the center wavelength. Pixel counts from the recorded camera image from each pixel indicate the intensity of light the respective wavelength range. This technology is rampant in the industry, where many companies are now implementing smart spectrometers that are highly consumer centric, like the SCiO by Consumer Physics, Israel.

Recently, several research groups, like those led by Dr. A Stern (Ben-Gurion University of the Negev, Israel) and Dr. Kevin Kelly (Rice University, USA), have uniquely and unconventionally applied computational techniques to spectrometry. Stating that most chemical spectra for the purposes of optical spectrometry are sparse in any given domain, they apply compressive sensing to reconstruct the spectrum. Over the past five years, they have proposed many techniques for generating the sensing matrix for such an inverse problem. These range from pattern generation using digital mirror devices, to that formed by changing the refractive index of spacer in a traditional Fabry Perot cavity through phase retardation. The solution of Etalon Array Reconstructive Spectrometry by the Zhaowei Liu group at UC San Diego aims at providing technique for high performance ultracompact spectrometers.

References and Acknowledgements

1. Andrei Tokmakoff, 5.33 *Introduction to Spectroscopy*, MIT OpenCourseWare Lecture Notes.
2. Nicholas C. Thomas, *The Early History of Spectroscopy*, J. Chem. Edu, Vol. 68 No. 8, Pg 631-634 (1991).
3. Newton, I., *Opticks* (Smith & Walford, 1704).
4. J. von Fraunhofer and W. H. Wollaston, J. S. Ames ed., *Prismatic and Diffraction Spectra* (Harper & Brothers 1898).

5. G. Kirchhoff, *On the relation between the radiating and absorbing powers of different bodies for light and heat*, The London, Edinburgh, and Dublin Philosophical Magazine and Journal of Science, 20:130, 1-21 (1860).
 6. Ingle, J.D. Jr. and Crouch, S.R. *Spectrochemical analysis*, (United States: Prentice Hall College Book Division, 1988).
 7. MIT Spectroscopy Lab: *List of Nobel Prizes in Spectroscopy*.
 8. David Ball, *Basics of Spectroscopy*, SPIE Tutorial Texts (SPIE Digital Library, 2001)
 9. A. J. Gordon, R. A. Ford, *The Chemist's Companion* (John Wiley & Sons, New York, 1972)
 10. P. R Griffiths and J. A. de Haseth, *Fourier Transform Infrared Spectroscopy*, (Wiley-Interscience, New York, 1986).
 11. Pavia, Donald L., Gary M. Lampman, and George S. Kriz, *Introduction to spectroscopy: a guide for students of organic chemistry*, Philadelphia: W.B. Saunders Co. (1979)
 12. R. G. Bingham, *Grating Spectrometers and Spectrographs Re-examined*, Q. Jl. No 4, Royal Astronomical Society 20, Pg. 395-421 (1979).
 13. Jacquinet P, The luminosity of spectrometers with prisms, gratings, or Fabry-Perot etalons J. Opt. Soc. Am. 44 761 (1954).
 14. J. Hearnshaw, *Astronomical Spectrographs and Their History* (Cambridge Univ. Press, 2009).
-

Etalon Array Reconstructive Spectrometry

The Complex Filter Array.

1. Overview

Fundamentals of EARS. Comparison with traditional spectrometric systems.

To spectroscopically probe a sample over a chosen spectrum range of interest, a spectral light measurement system is necessary, which must include a wavelength selection/splitting component. Spatial to spectral mapping based on diffractive or dispersive optical elements is often implemented, as previously discussed in Chapter Two. These conventionally include the prism and the diffraction grating¹. Alternate methods also include spectral filtering using tunable narrow-band spectral filters^{2,3}, like Fabry Perot (FP) interferometers and acousto-optic tunable filters (AOTF), or interferometric analysis in spectral domain, like the Fourier Transform Infrared Spectrometer (FTIR)⁴. For dispersive components such as the prism and grating, it is imperative that for high resolution spectral

analysis, the propagation distance from the component to the detector be long (inversely scales with optical path length). This need inevitably attributes the bulky form factor of spectrometers and does not permit integration with the detector module⁵.

A coping technology is the use of filter arrays⁶, which is a series of absorption or interference filters that selectively transmit desired spectral components and block the rest through an absorption or interference process. This has proven to be particularly useful as the array can be fabricated directly on top of the camera sensor array, yielding quick measurements and compact overall form factor with no light propagation necessary. Some variations to the filter-based method comprise of filter-wheels⁷ and tilting filters⁸, where discrete wavelengths can be selected by rotating through different filters or changing the incident angle of light respectively. Therefore, filter-based spectrometry has often been presented as a very popular procedure aiding in compactness of spectrometers, only, it has three chief limitations:

- a. High spectral resolution would demand a larger number of narrowband filters (N) in the array, which not only poses fabrication complexity but also reduces the efficiency of light that reaches the detector.
- b. Each filter also blocks out light, resulting in a further decrease in efficiency at the detector pixel due to a low-level signal ($1/N^2$). This makes high resolution spectrometry challenging.

- c. Requires high number of measurements for direct one-to-one spectral mapping, often also posing a need for a larger detector array.

Filters are then employed for spectroscopy only when the application and the signal to be measured is known to overcome these fundamental limitations.

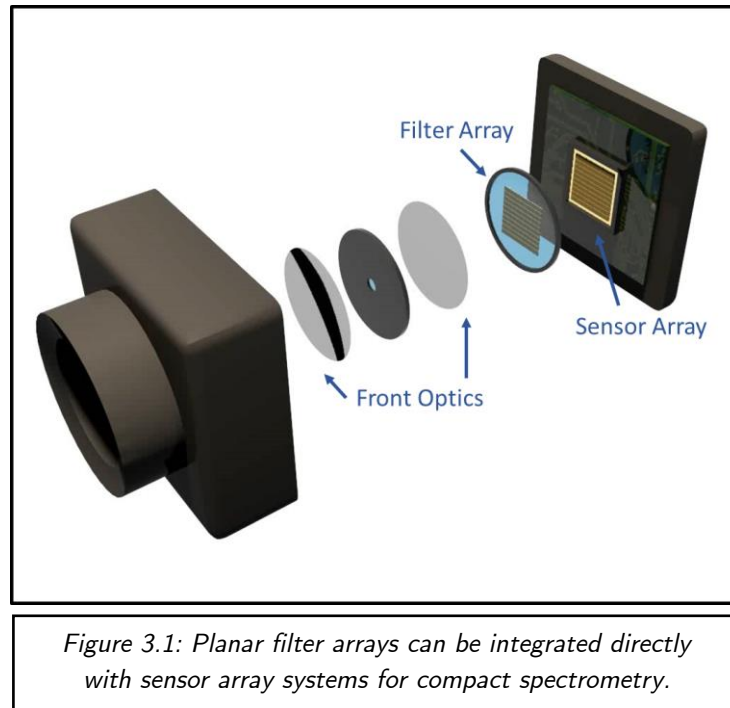


Figure 3.1: Planar filter arrays can be integrated directly with sensor array systems for compact spectrometry.

In comparison to such direct measurements thereby conducted, compressive sensing⁹ algorithms offer to preserve high fidelity of spectral signals by taking far fewer measurements, given some technical constraints on both the sensing system and the signal of interest. For CS based reconstructive spectrometry, the following is established:

- a. Measurements, M , conducted are indirect, encoded and multiplexed. This implies that each measurement consists of information by multiple wavelengths.
- b. If the total number of direct measurements is N , CS can achieve reconstruction with $M < N$, at the cost of post-processing after acquisition through a detector.
- c. A priori information about the signal is necessary, such that it can be represented sparsely in a chosen transformed basis (example: Fourier, Wavelet, Hadamard, etc.).
- d. The sensing matrix must consist of non-zero off diagonal elements, unlike direct ways of spectral mapping, which also represents the linear projections of the signal.
- e. Reconstruction is then possible using a best-fit algorithm, which in the case of EARS is the l_1 norm minimization.

In our method of Etalon Array Reconstructive Spectrometry¹⁰, or EARS, the incident light is uniquely encoded using an array of optical filters or etalons (FP cavities) that acts as a complex filter array for multiplexed measurements. Each cavity is characterized by linearly varying optical thicknesses, akin to a staircase structure, and therefore transmits a different intensity value per wavelength. Since the characteristic transmission through each of the

cavities is known, the spectral encryption denotes the known sensing matrix used for reconstruction. Such a geometry has no moving parts and adds robustness to the compact spectrometer design. The computational advantage enhances the design flexibility as the number of measurements is no longer tied to the number of filters (or sensors) for spectrum detection. In other words, the amount of light transmitted through an etalon is independent of the desired spectral resolution, providing SNR and speed advantages.

EARS is a computational, complex, camera-based spectrometric method that yields ultracompact, inexpensive, robust, fixed spectrometer design with broadband, high-resolution, fast spectral acquisition capability.

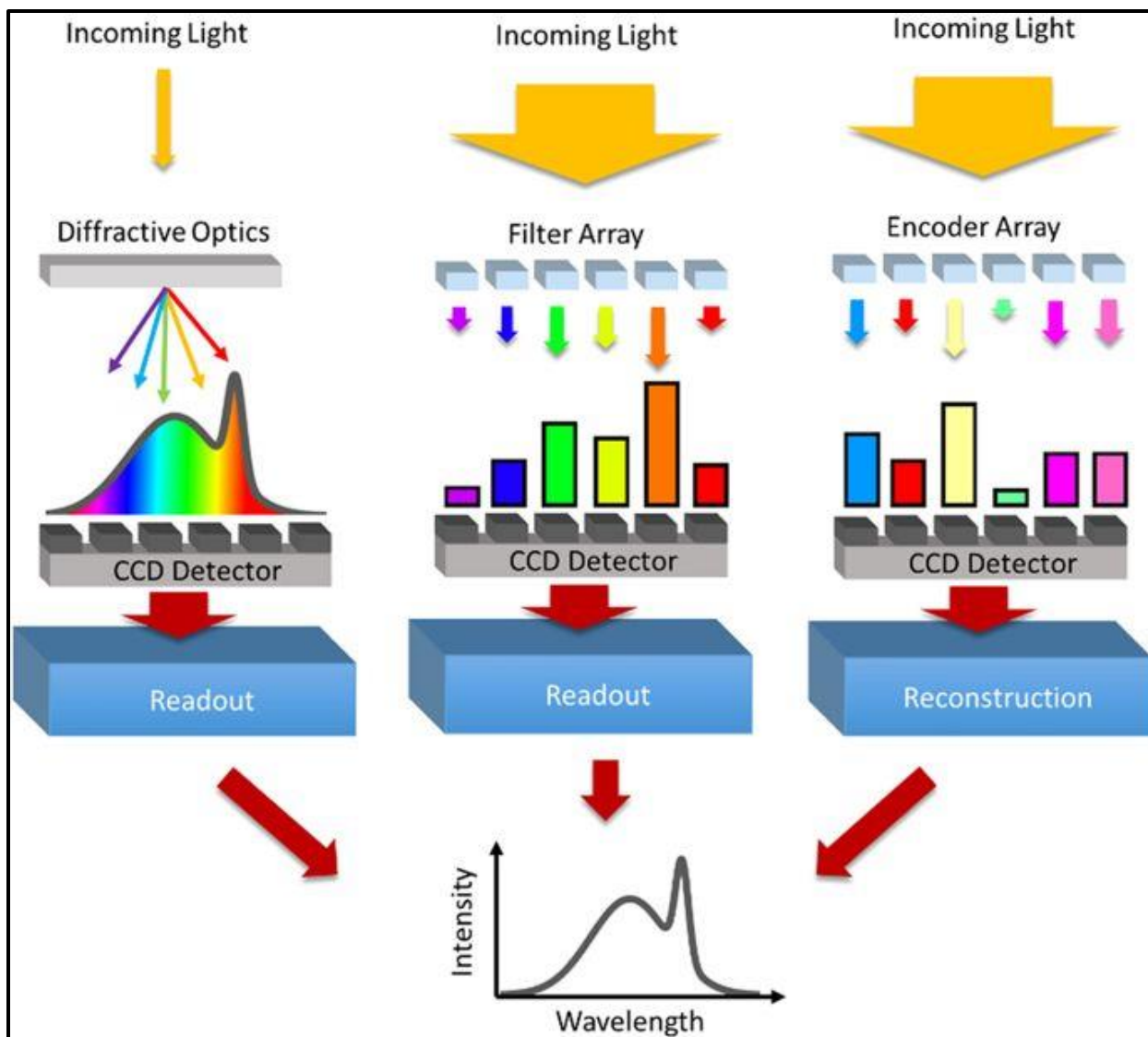


Figure 3.2: Comparison of conventional spectrometric techniques with reconstructive spectrometry (far right). The schematic represents different measurements schemes in which the spectrum is recovered.

2. Operation

Technical Perspective. Significance of the etalon array. Sensing matrix generation.

Etalon Array Fabrication. Experimental setup.

Applying a sensing pattern in CS spectrometry implies that the light distribution must essentially be modulated and multiplexed⁹. The choice of etalon array as the encoding structure can be explained primarily due to its resonance modulating transmission. A single etalon consists of two parallel, partially reflective mirrors with reflectivity R , separated by an optically transparent spacer material of index n . When light of wavelength λ is incident normally on the first surface, it gets trapped in the resonator cavity, incurring multiple reflections back and forth from the two surfaces, and escapes the other surface at certain resonant wavelengths. Figure 3.3 delineates the fundamentals of the etalon.

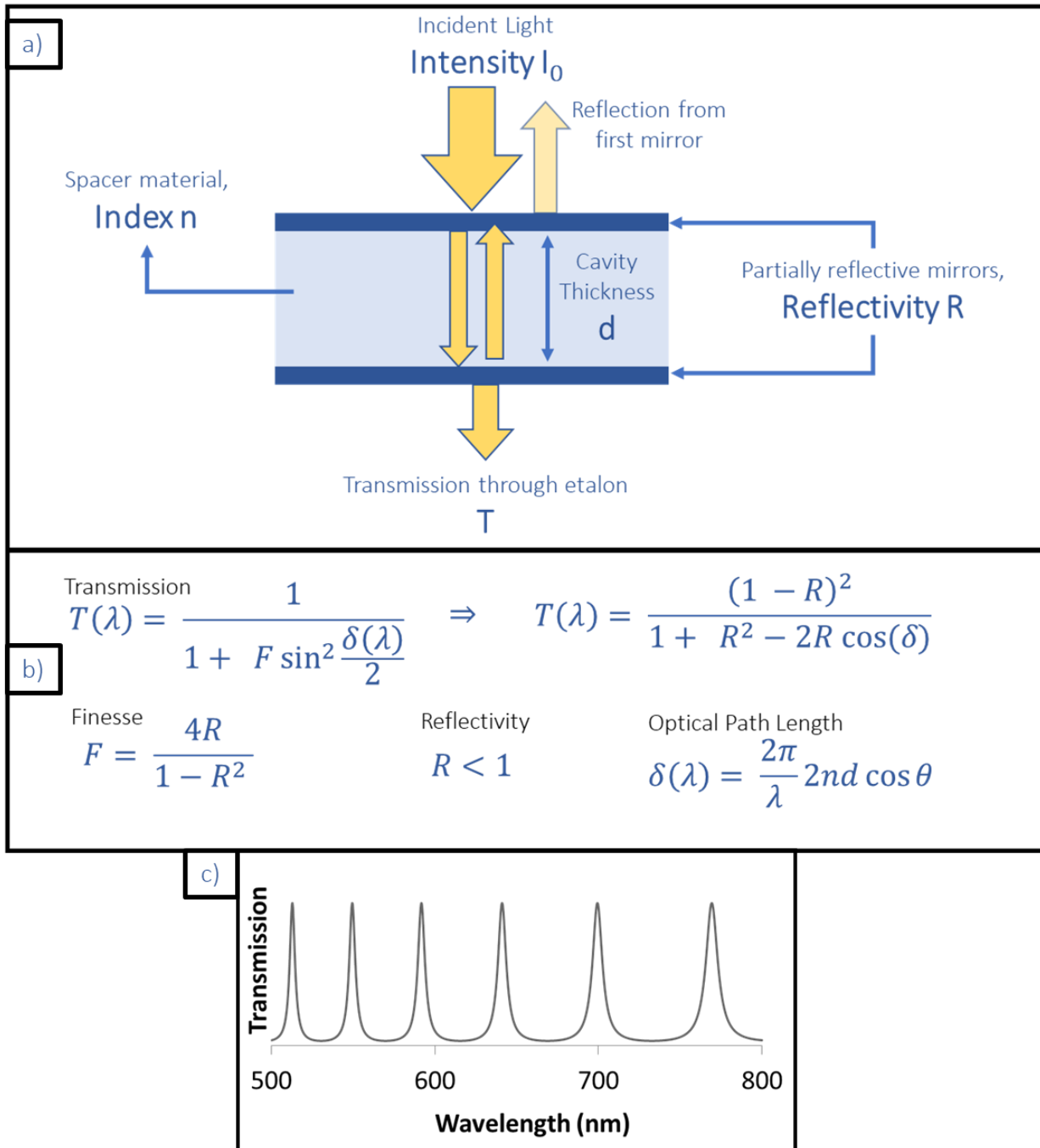


Figure 3.3: Etalon Fundamentals. (a) Schematic of a typical optical resonator/etalon, (b) Underlying theory, (c) Transmission spectrum of the etalon for a given optical path length, δ , and reflectivity, R .

The transmission spectra through an etalon can be described as a series of peaks. The spectral position of these transmission maxima can be controlled by changing the optical path length within the etalon. In the paraxial case, i.e. for $\theta = 0^\circ$, this becomes a product of refractive index n , and cavity thickness d . For an etalon array, we develop a staircase structure where each cavity is linearly increasing in thickness, d for the same spacer material (n). Figure 3.4 shows the correlation of changing d with changing spectral peak locations for two different etalons. Figure 3.5 encapsulates the essence of the etalon array structure, along with a mathematical understanding of the CS reconstruction. Typically, for high resolution spectroscopy, we require the Finesse (F) or the equivalent Q-factor of the etalon transmission to be as high as possible so that the resulting peaks are narrow. Narrow peaks maintain greater incoherence between sets of measurements, which is favorable for optimal CS conditions (discussed in the section on Optimization). However, the peaks also need to be wide enough to sufficiently cover each wavelength. An optimal R therefore needs to be established. Spectral modulation using the cavity array is made intuitive by Figure 3.6.

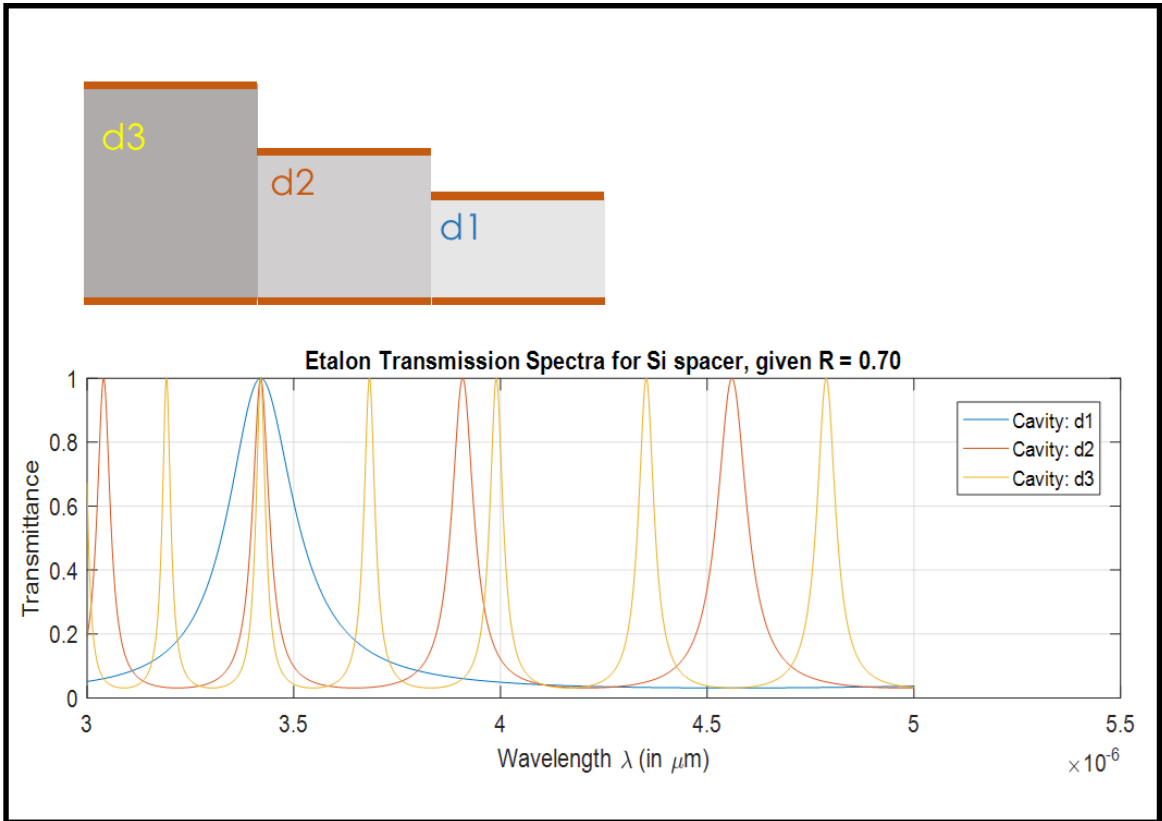


Figure 3.4: Impact of cavity thickness on etalon transmission

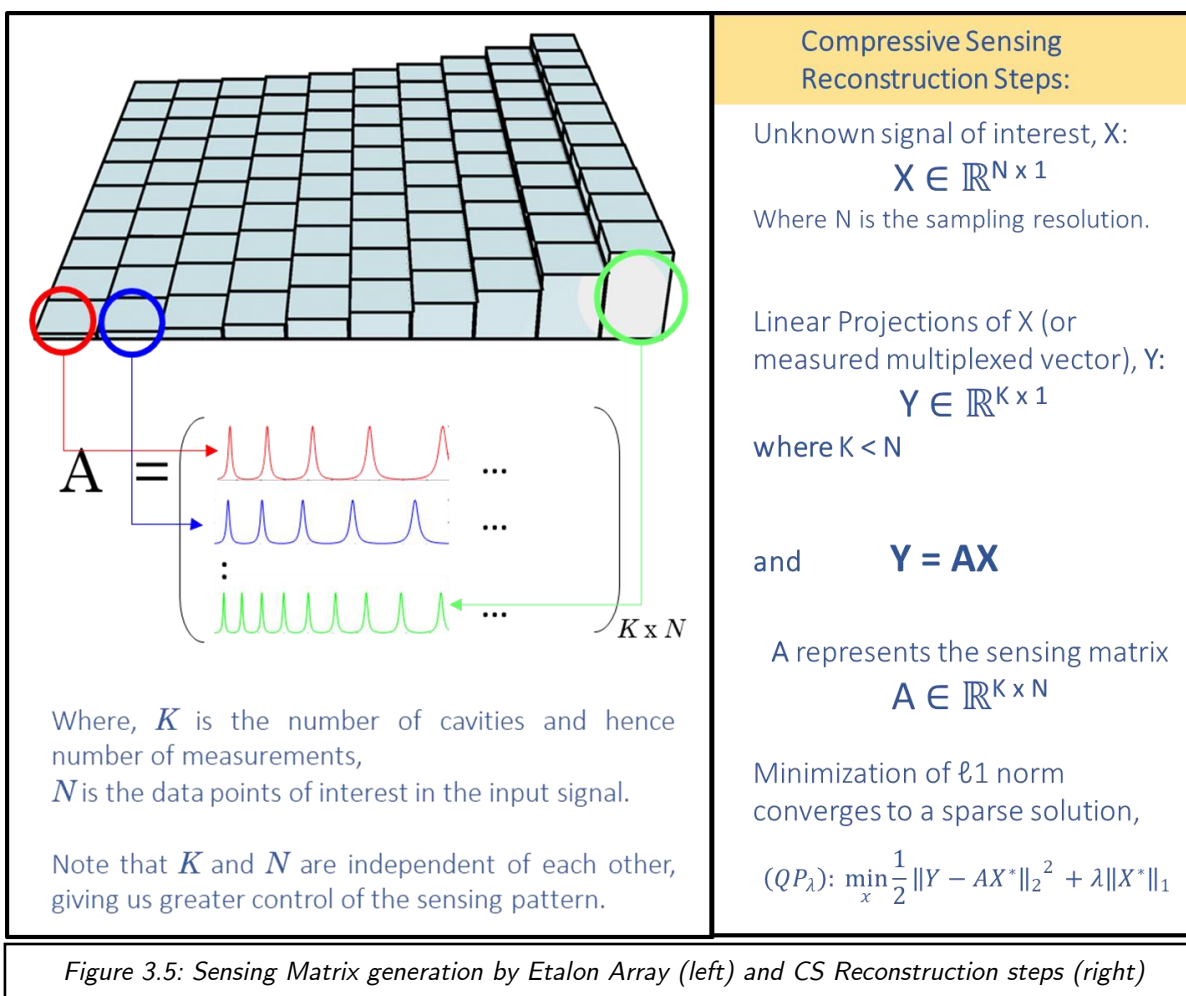


Figure 3.5: Sensing Matrix generation by Etalon Array (left) and CS Reconstruction steps (right)

Fabricating the etalon array¹⁰ incorporates standard lithographic techniques, with the most prominent procedure being electron beam lithography. Alternate methods of nanoimprinting can also be implemented. The materials used greatly depend on the optical window for transmission in the wavelength range of choice. For VIS-NIR spectrometry, a silver mirror coating (30 nm) is sputtered on a glass substrate, on which a protective lining of 700 nm SiO₂ is deposited via plasma enhanced CVD. The thickness of silver is ascertained based

on the desired reflectivity (or Q-factor) for lowest coherence parameter. For generating the step structure of varying thicknesses from 20 nm to 2 μm , a 2.8 μm thick PMMA was spin-coated, and to make the sample conductive for e-beam lithography, a 2.5 μm Au layer was sputtered on the PMMA. A grid of 10x10 squares (500 μm by 500 μm) were exposed to a varying e-beam doses at 10 keV. The Au is then etched away using potassium iodide and the PMMA is developed in methyl isobutyl ketone solution for 5 minutes and is then rinsed with isopropyl alcohol. After drying the sample with nitrogen, the second silver mirror is sputtered on top after also depositing a thin protective layer of SiO_2 . The optical length variation including SiO_2 then is 1.5 to 3.5 μm . Note: the development of etalon array structure for the far infrared is a matter of ongoing work, considering a polymer resist such as PMMA is not completely transparent in that region.

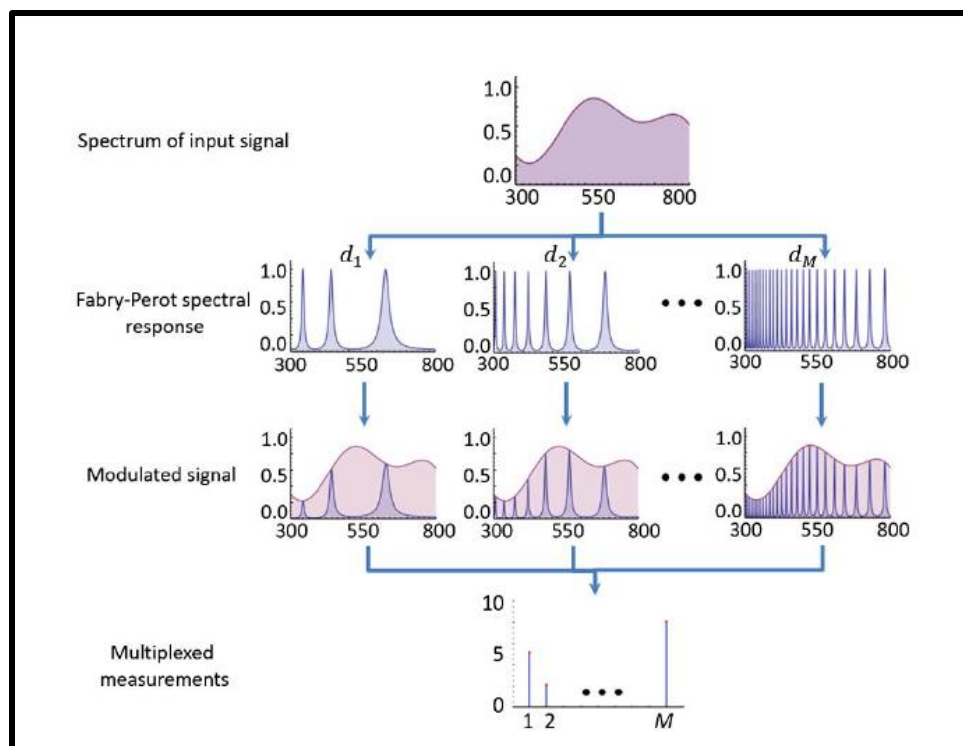


Figure 3.6: Spectral Resonance Modulation using Fabry Perot cavities¹¹

The experimental setup for EARS, shown in the schematic figure 3.7, is broken down into three crucial steps: a. Calibration, b. Multiplexed Signal Acquisition, and c. Computational Reconstruction. The overall setup is identical in many ways to a conventional filter array spectrometer. Two sources are used to test the EARS method. First, a broadband supercontinuum laser light source illuminates the etalon array by passing through a two-objective system. The etalon array is placed in the conjugate image plane of the CCD Camera and a slit is used to accurately measure transmission through each etalon individually by sending the signal to a grating spectrometer, essential for calibration. At the end of this step,

the sensing matrix is generated. In the proof-of-concept experiment, we first attempt reconstruction of several spectra of when supercontinuum laser light passes through a tunable bandpass filter at chosen central wavelengths. Then, we measure the spectra of known laser sources (linewidth of the order of ~ 1 nm, hence extremely narrowband). The results are discussed in the next section.

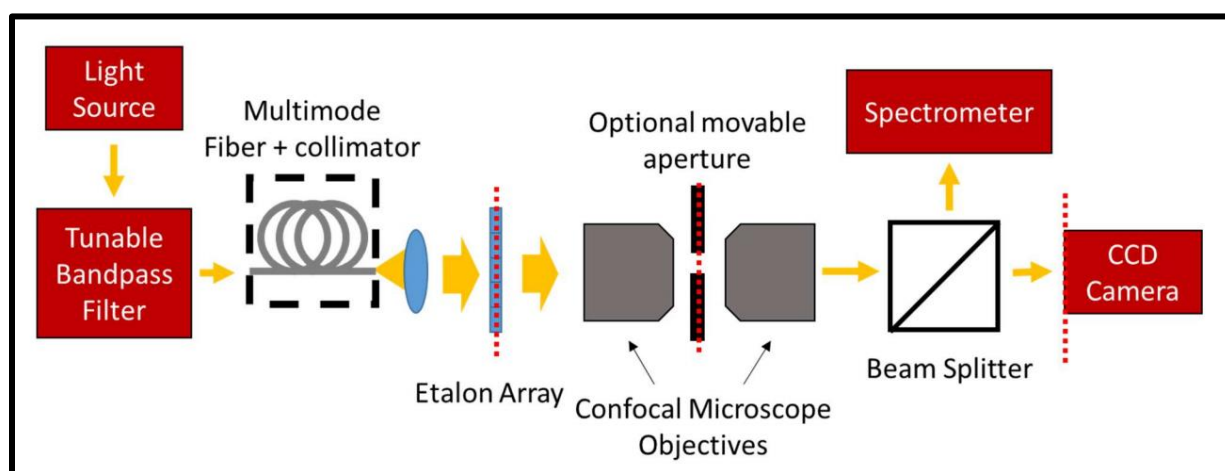


Figure 3.7: Schematic of the experimental setup for practical EARS¹⁰

3. Outcome

Measurement and algorithmic reconstruction results. Inferences.

An important condition for the sensing matrix in CS spectrometric reconstruction is to have non-zero odd diagonal elements, or linear projections, in the given basis. From the

calibration, we accurately measure the transmission through each etalon such that every row in the sensing matrix (for K measurements), is populated with the spectrum of that cavity. For the proof of concept measurement, we used another grating spectrometer as a reference; however, alternative methods of calibration exist. One such method involves using multiple inexpensive laser diodes spanning the visible wavelengths (like Red, Green or Blue) to sample the transmission spectra of the device. The respective transmission can be recorded and retraced computationally to fit the spectral response for an approximate cavity thickness. See figure 3.8 for an image of the sensing pattern of the etalon array.

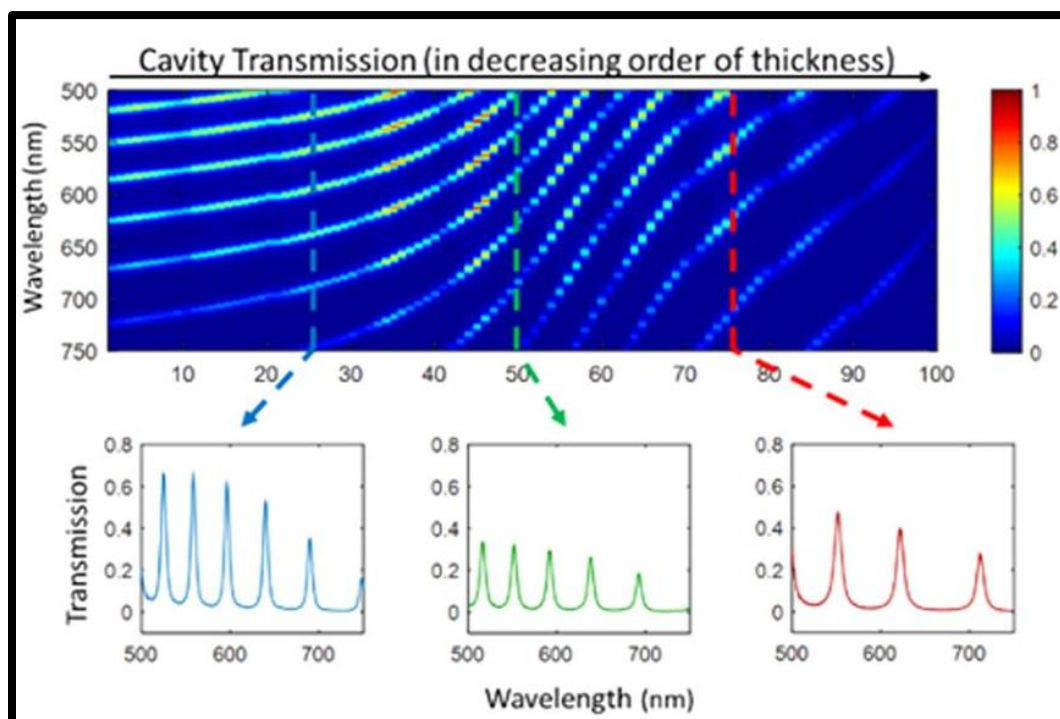


Figure 3.8: Visualizing the sensing matrix created by the etalon array.

Two different sources were used to test the working of the EARS. Results are shown in figure 3.9. The tunable bandpass filter that filters supercontinuum laser light gives a series of broadband signals that CS reconstruction recovers convincingly. The other signals that EARS recovers are laser spectra. This specific source is resourcefully used to show that when the signal is particularly sparse in the domain, as in a laser spectrum (all elements are mostly zero, monochromaticity), CS reconstruction works with greater accuracy and higher resolution. Alternatively, if more information about the signal is known (such that it can be represented in a sparse basis) or if known spectral features can be found only in the wavelength range of interest (using bandpass filters), CS reconstruction would be a much better candidate for robust, versatile spectroscopy. One must also note that the signal to noise ratio is critical in CS reconstruction. If the fidelity of the measurement signal is compromised, the reconstruction is error-prone, and often breaks the sparsity limit. While the sparsity limit can be previously calculated and adjusted in the experiment, or incorporated in the minimization algorithm accordingly, higher resolution is possible only with high SNR. Some array parameters can be varied to achieve this too. More on this is covered in optimization. However, with resolution independent of the number of measurements, there is added flexibility to the parameters in the process.

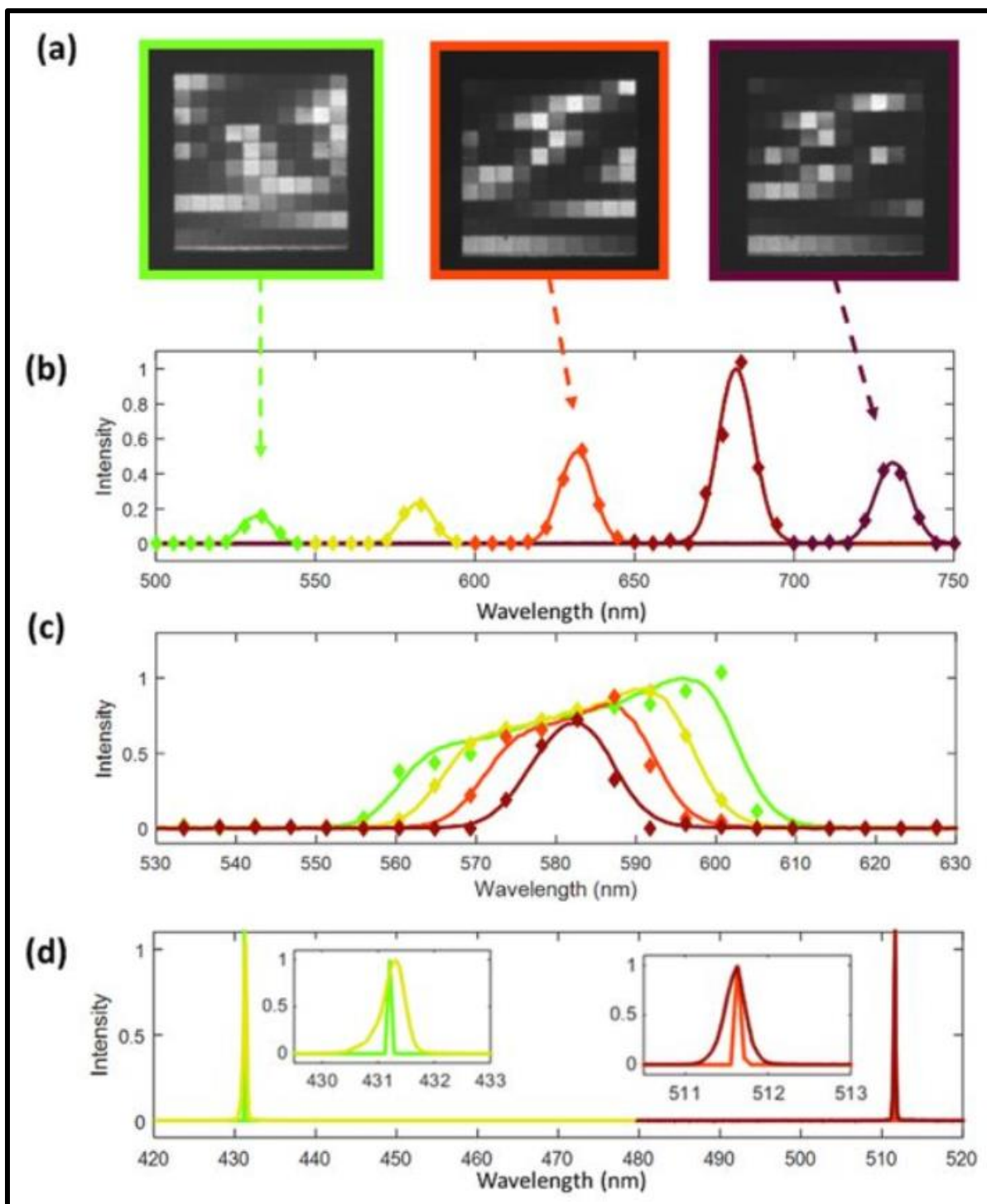


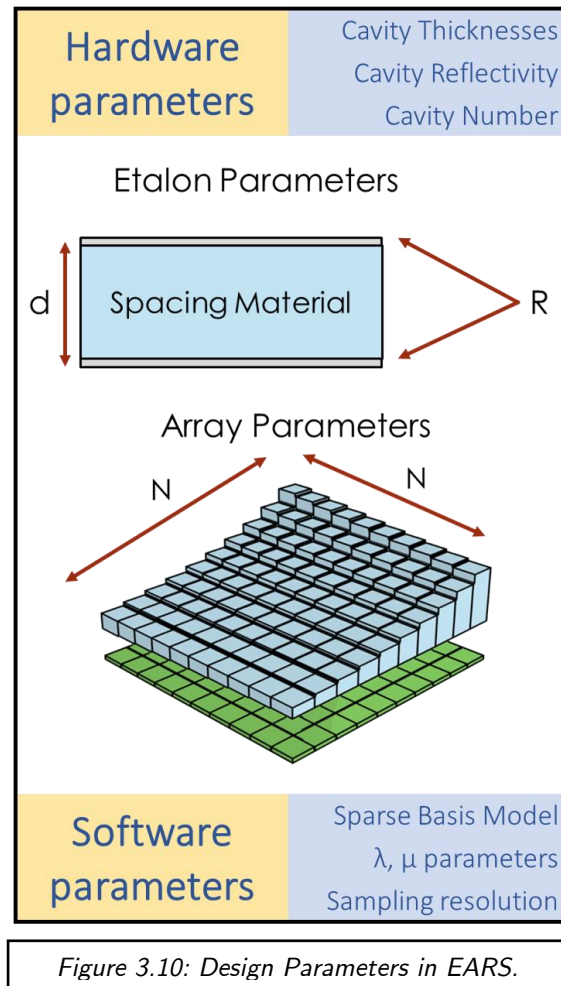
Figure 3.9: (a) Etalon array illumination using supercontinuum laser with tunable bandpass filters. (b) spectrum reconstruction results, (c) broadband spectrum reconstruction, (d) laser spectrum reconstruction¹⁰

4. Design Analysis

Parameters for CS reconstruction. Sparsity limits. Figures of merit for optimal reconstruction. Array design for various wavelength ranges. Rough guideline. Special application of EARS in the Mid infrared.

To check for the fidelity of the reconstruction strategy deployed in this computational spectrometry method, a commonly used metric is the minimum mean squared error (MMSE) or more appropriately, for standard deviation frame of reference, the root mean squared error (RMSE). The goal is to have the least amount of error, implying RMSE as close to 0 as possible, even when subjected to noisy environments. This would imply that the spectrum is accurately recovered under the compressive sensing scheme. In other words, RMSE is an indicator of the *reconstruction performance*.

In a collaborative effort acknowledged in this chapter, the study on design analysis of both hardware and software parameters for minimum RMSE is done bearing in mind a mid-infrared working regime, specifically applied to chemical sensing. However, the general trend can be also translated to other parts of the spectrum. Knowing that desired spectrometry deliverables are high resolution, high bandwidth and sensitivity, we can explore our parameter space, as shown in the figure 3.10 below.



The strategy for design analysis is an iterative process which is carefully considered step by step. The desired spectrometric specifications are prioritized as 1. Resolution, 2. Bandwidth, and 3. Sensitivity. It must also be noted here that sensitivity is greatly dependent on noise level in the system, and therefore an SNR analysis is implemented. Poor SNR coping mechanisms are also introduced. The complete procedure is explained in figure 3.11.

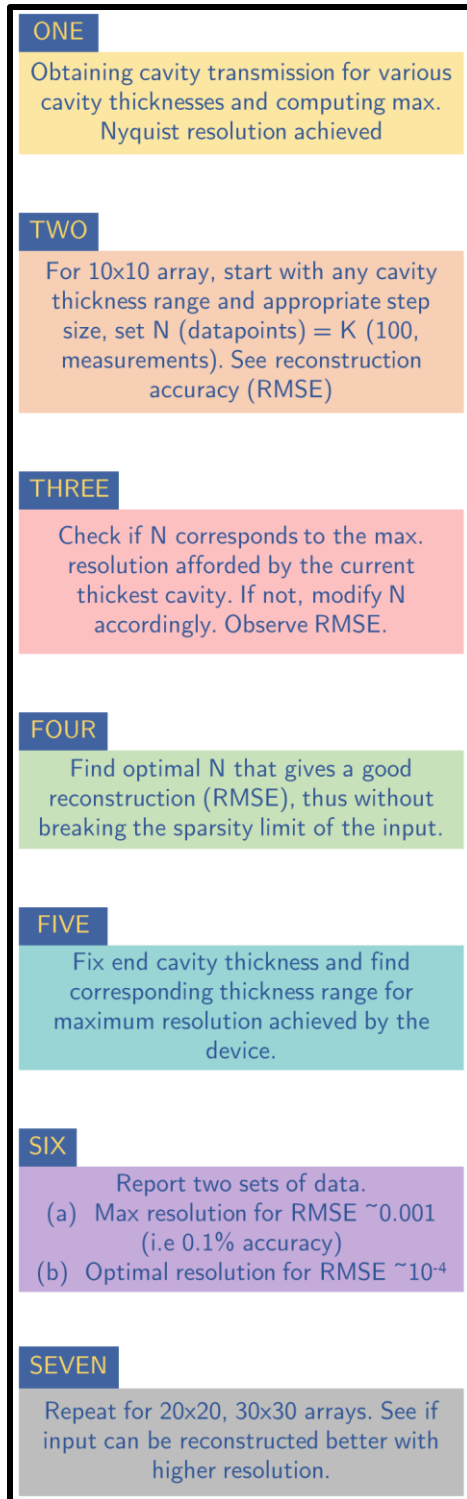


Figure 3.11: EARS Design Procedure

The story of design analysis is followed by table 2 that summarizes the parameter requirements and observations. We begin by ascertaining the hardware capabilities. Since we have complete control over the etalon array, we can design for the configuration that yields the lowest RMSE. We know that if reflectivity (R) of the etalon is high, the resulting peaks would be extremely narrow, providing high contrast and reduced correlation between measurements, also represented as coherence parameter (μ). However, we also want to measure across sufficient wavelengths so that there is enough information about each. The optimal R for a 20 nm silver mirror and still low coherence was found to be between 0.7 and 0.8. The thickness of the largest cavity is important of two reasons: a. it governs an estimate of the maximum resolution achievable by the system, given as the FWHM, and b. the transmission spectrum becomes denser as the thickness increases, which would be attributed to a high resolution due to more closely separated maximas. Graph delineates a relation between maximum resolution with increasing thickness values. Combined with a larger thickness range (of the order of 100 μm or greater), our sensing matrix would be more unique. If the thicknesses of the cavities have predefined constraints, the index of the spacer could also be increased. However, it is always recommended to be cautious of dispersion and loss through a thick cavity due to imaginary component of refractive index, or simply, loss. In this study, the dispersion is quantified using Sellmeier's equation. It may also be necessary to calibrate for temperature in the mid infrared region of operation.

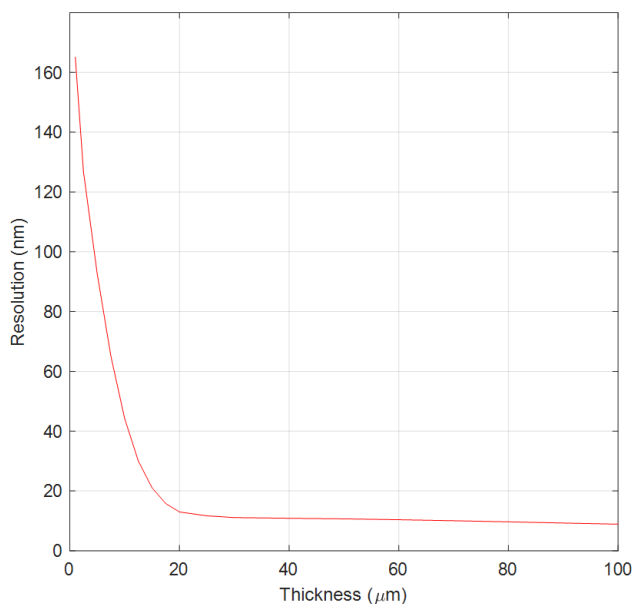


Figure 3.12: Nyquist Resolution (Sampling rate) afforded by different cavity

While the optimal hardware is determined by a series of computations, keeping a given configuration of the etalon array and altering the software parameters is considerably less intensive. Setting a high number of measurements (high number of cavities) is favorable. More measurements mean more data points, which in turn implies more achievable resolution, since we are measuring a greater number of pixels. This however is a trade off with sensitivity, as light is spread across more number of complex etalon filters. The sampling resolution (N) of the spectrum to be reconstructed can be increased, but this must be appropriately supported by an increase in the number of measurements (K). Sparsity of the signal breaks easily if the difference between N and K is too large. Another reason for sparsity break is if the algorithm

is attempting to recover a signal with too many non-zero elements. For this, the coping strategy would be to represent this signal in a basis in which it is sparse. For example, if a chemical identification application is so desired as to find the existence of the chemical in a compound mix, the basis of representation can be the spectral signature of the signal itself. The following section on Opportunity would include the results for such an application.

Table 3.1: Design Parameters used for the Mid IR Wavelength

Parameter	Characteristics	Notes
Spacing Material	Silicon (n = 3.42)	Transparent to light in 3 to 5 μm
Reflectors	Silver/Aluminum (R = 0.7)	Reflectivity fixed for all cavities at 0.7.
Cavity Thickness	10 to 100 μm , step size of 100 nm Can be thicker (~200 μm), for more rigidity. Note, thicker cavities may introduce greater attenuation and angle-sensitivity.	Larger thickness range attributes more accurate reconstruction, mapping both the low and high resolution details of the input spectrum.
Array Size	30 by 30 array (900 cavities) Can be varied accordingly to suit application.	Greater number of pixels, greater information about the signal. Hence more accurate reconstruction

Rough Guideline

$$\left(\begin{array}{l} \text{Thickness} \\ \text{Range, } d \end{array} \right) \times \left(\begin{array}{l} \text{No. of Etalons} \\ \text{in Array, } K \end{array} \right) = \frac{\text{const.}}{\text{RMSE}}$$

*at a given sampling rate (Nyquist resolution)

Figure 3.13: Handbook Formula for Spectrometer Design Parameters

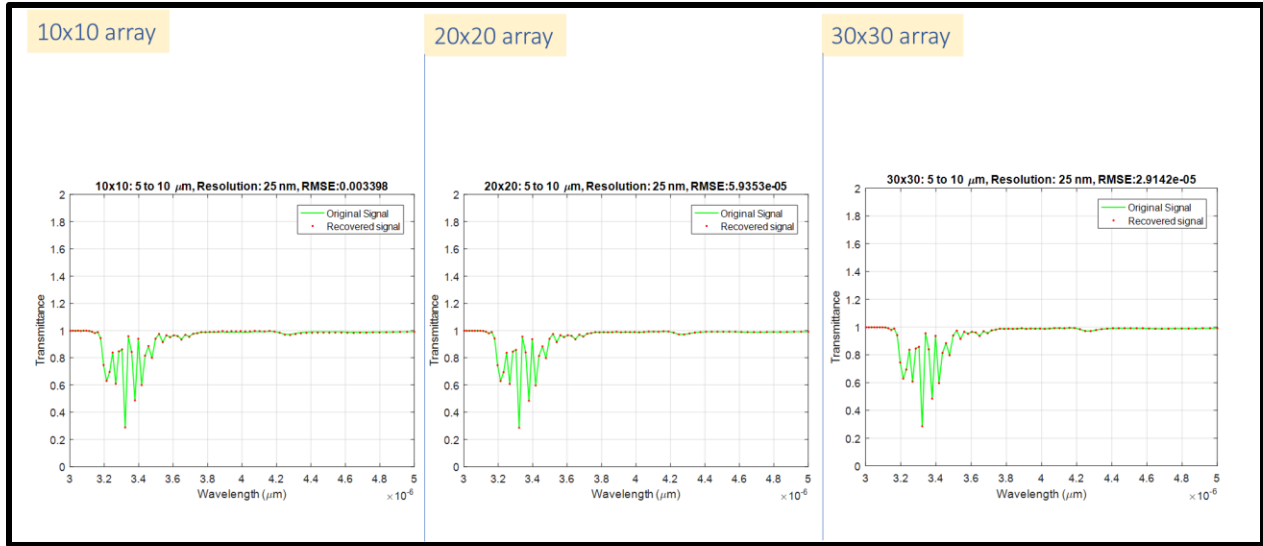


Figure 3.14: Better Reconstruction Performance with increasing number of cavities. At lower resolution (25 nm), 30x30 array gives two orders of improvement in reconstruction as compared to 10x10 array for a smaller thickness range.

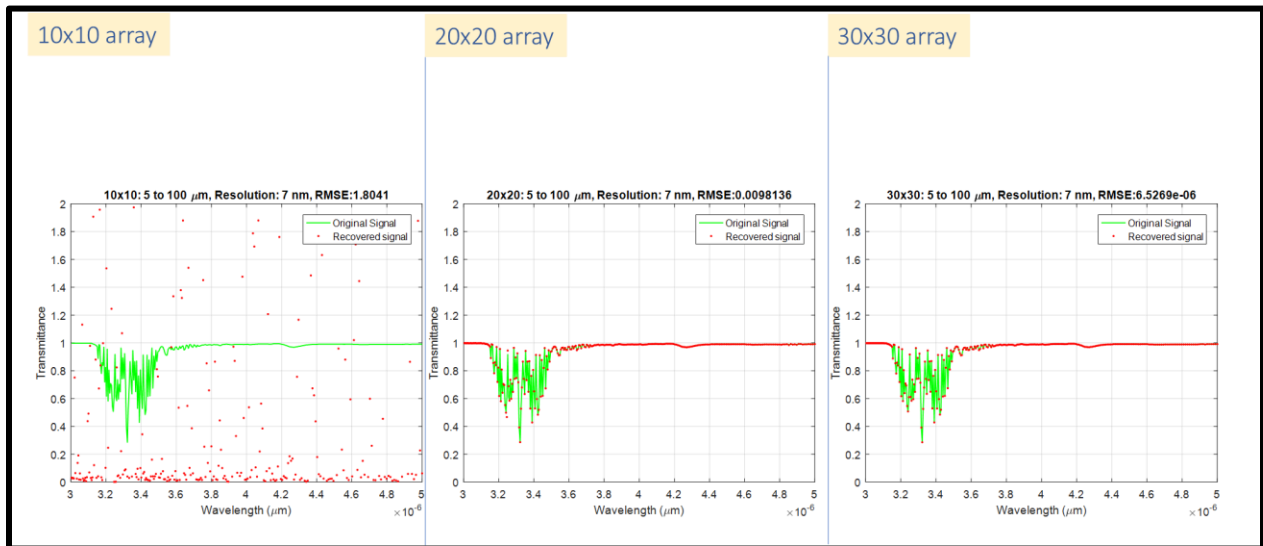


Figure 3.15: Better Reconstruction Performance with increasing number of cavities. At higher resolution (7 nm), 30x30 array gives six orders of improvement in reconstruction compared to 10x10 array as the sparsity breaks easily for the given thickness range.

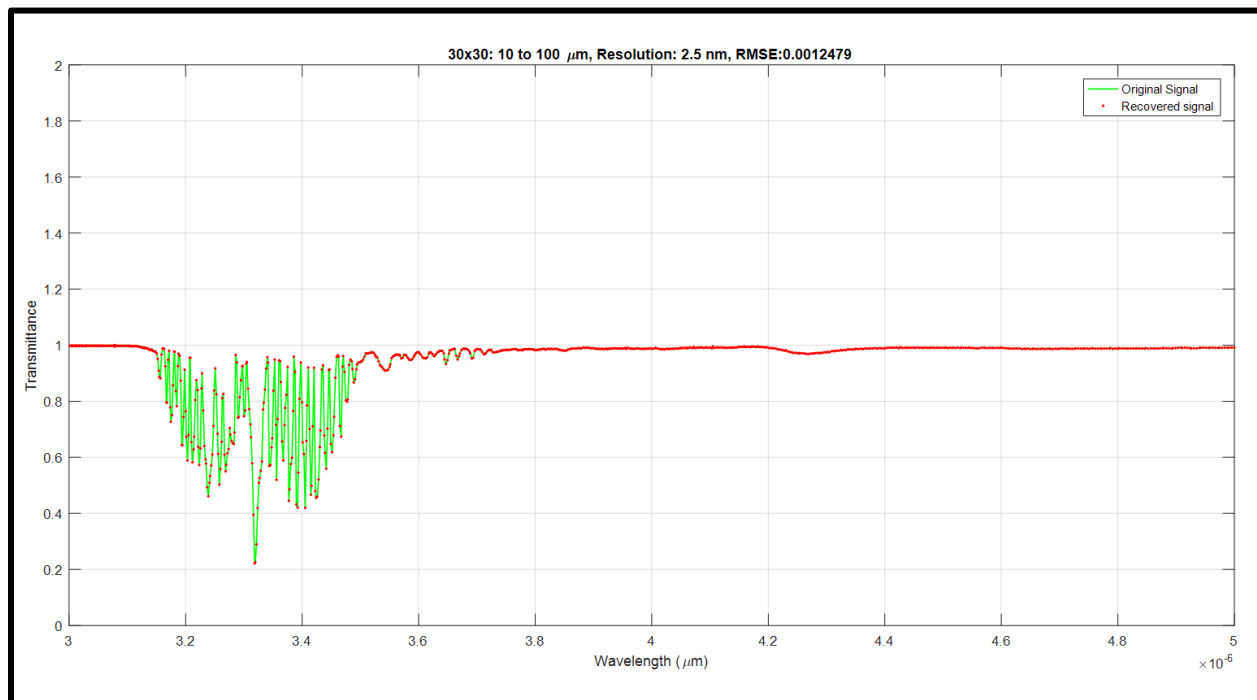


Figure 3.16: Best Configuration with the 30x30 array. Resolution of 2.5 nm is achieved in the MIR.

SNR is easily the most critical part of any detection and/or reconstruction system. Real world applications involve noisy measurements. One caveat of such an etalon array is that light incident on an etalon is mostly reflected, which already reduces the total intensity that reaches the detector. This imposes a stricter challenge on signal recovery with respect to a noise floor. Figure 3.17 analyzes the RMSE values attained post reconstructing as SNR increases subject to an additive white gaussian noise model. Intuitively, high SNR gives high quality recovery. Subsequent graphs compare the noise performance in different configurations.

A research study¹² on characterizing the different regions in a noise performance graph indicated its nuanced behavior in a compressive sensing system. This implies that the RMSE v/s SNR curve is never completely linear and can have unexplained trends owing to the measurement region it belongs to (high measurement = high K, low measurement = low K).

$$[Y] = [A][X] + w$$

Where Y is the measured output,
A is the known sensing matrix and
X is the spectrum to be reconstructed.

Let w be the additive measurement noise

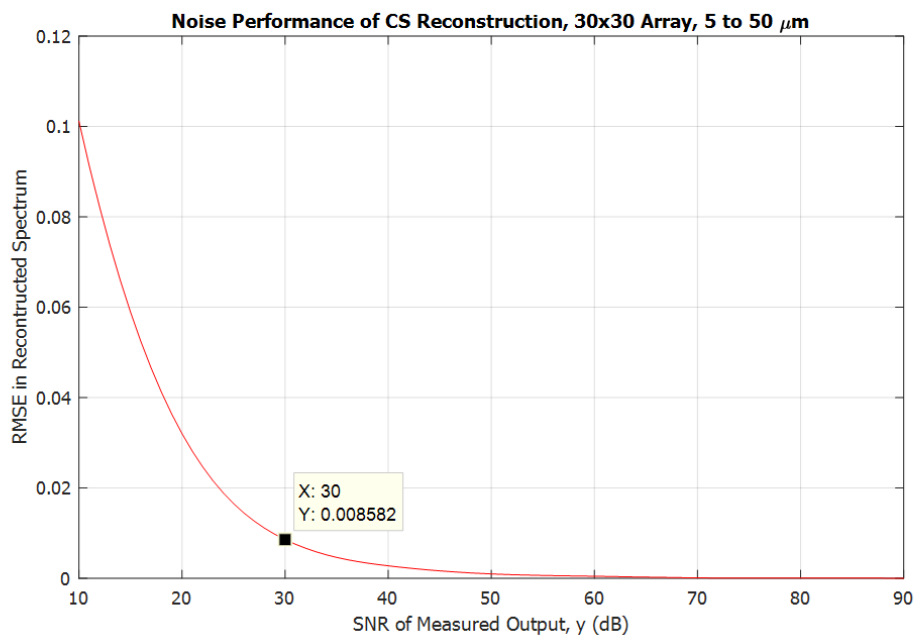


Figure 3.17: Reconstruction Performance with increasing Signal-to-Noise Ratio for an AWGN noise model.

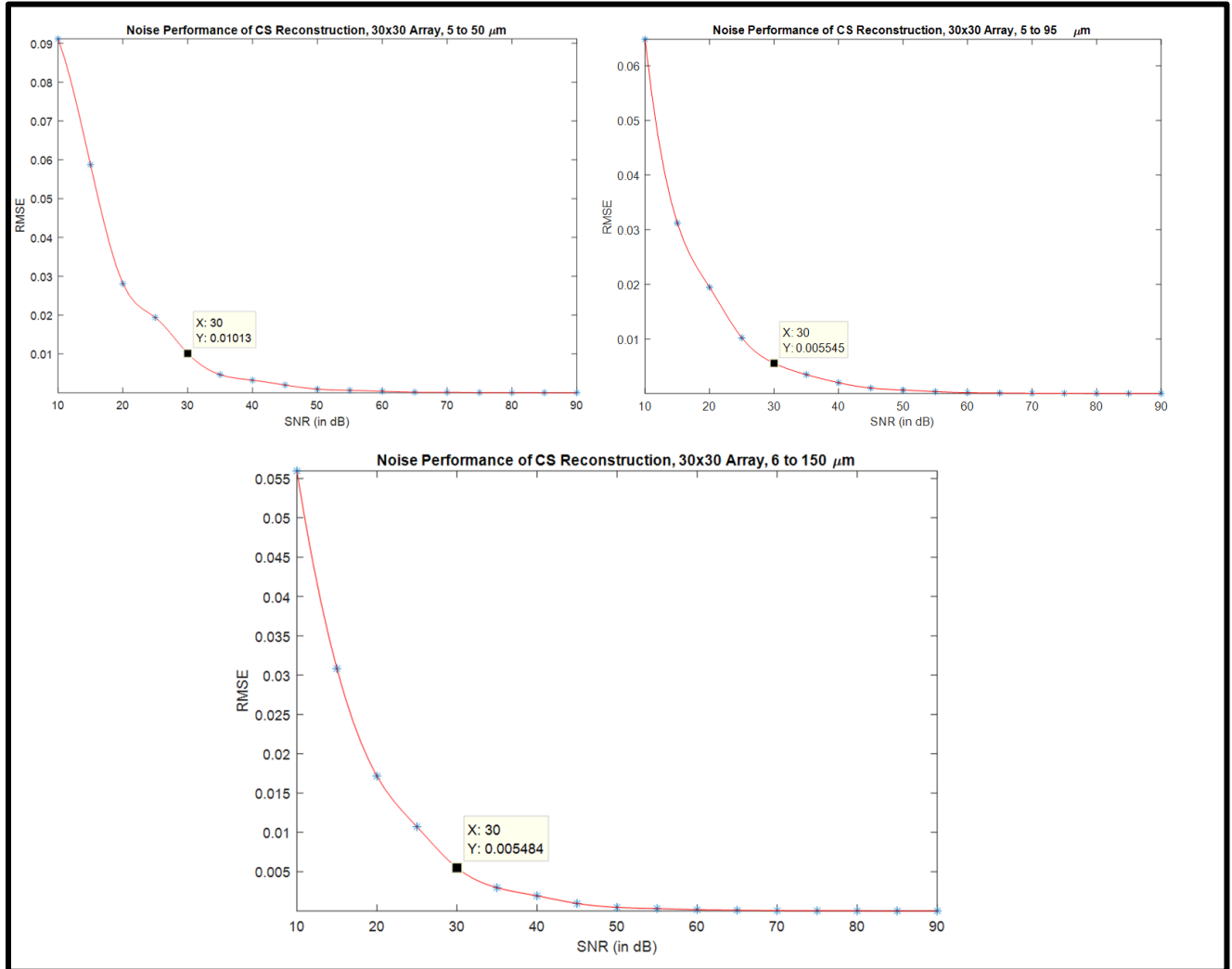


Figure 3.18: Reconstruction Performance v/s SNR with increasing cavity thickness range from 5 to 50 microns, 5 to 95 microns and 6 to 150 microns. 30 dB is an acceptable SNR limit to CS reconstruction as long as $RMSE < 1\%$, below which signal quality, hence reconstruction, degrades severely.

Several coping mechanisms for SNR are primarily based on a priori knowledge of the spectrum to be reconstructed, and are listed as under:

(a) Hard Threshold for Peak(s) Determination-

To extract specific spectrum features, such as characteristic peaks in a chemical spectrum, we can apply a hard threshold that enumerates the peaks and their spectral location, making the rest of the signal zero. This practice reduces the number of measurements thereby recovering the (highly sparse) peak values exactly, which can be confirmed by checking if the reconstruction is accurate within 5% of original signal and is true for at least 90% samples in question. Such a method is particularly useful in identifying chemical substances.

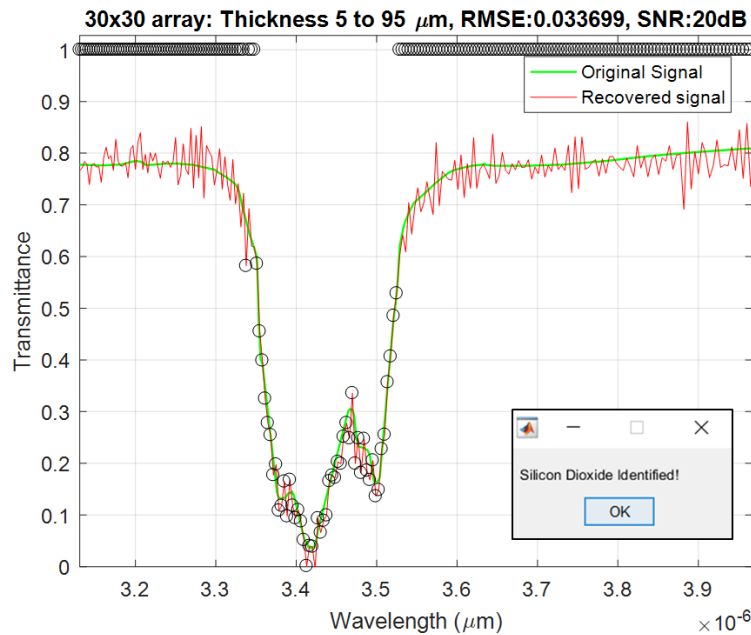


Figure 3.19: Hard Thresholding to extract specific spectrum features for reduced number of measurements.

(b) Adaptive Threshold for Peak Determination

Instead of applying a hard threshold, the peaks may be located by adaptively clustering the data points around peak values. 1-D adaptive thresholding can be applied to find samples around the peaks. This, again, reduces the number of measurements and decreases RMSE values.

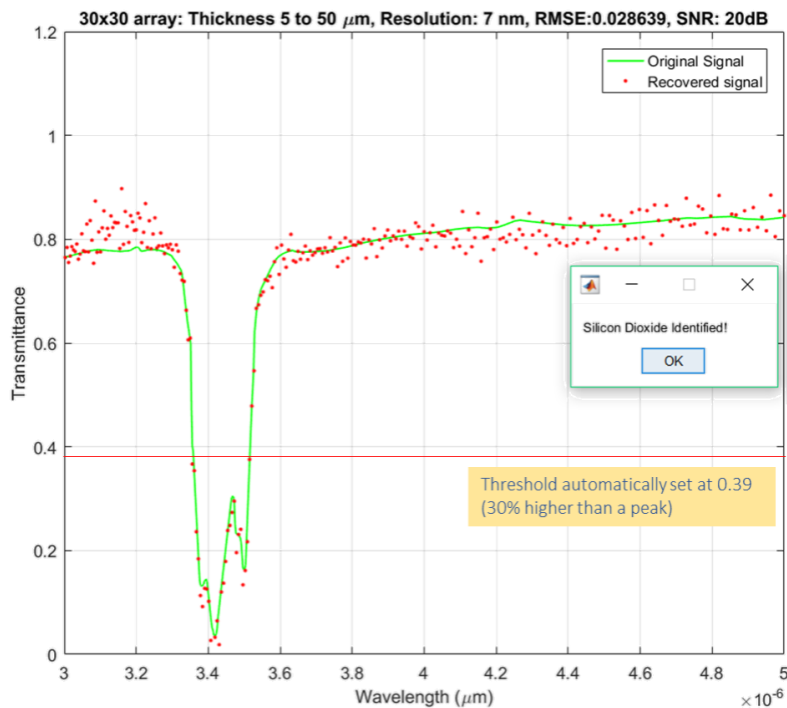


Figure 3.20: Adaptive Thresholding to extract specific spectrum features for reduced number of measurements for

(c) Reduced Regions of Interest:

Knowing the characteristic spectral signature with respect to unique features in said spectrum, bandpass filters can be applied to block out the wavelength regions where no such unique features exist. The number of measurements is reduced, which not only increases achievable resolution but also improves signal to noise ratio.

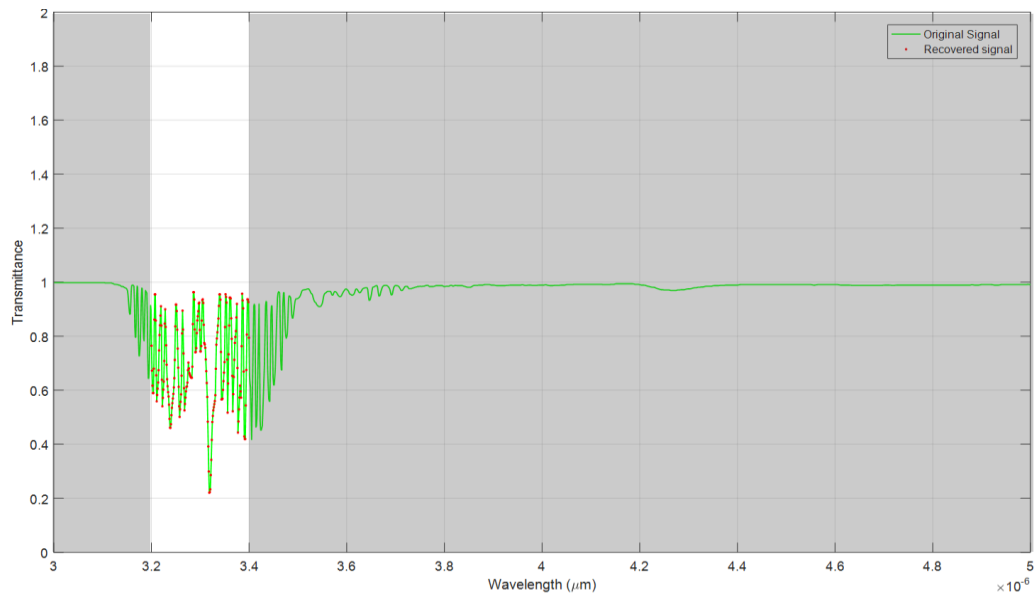


Figure 3.21: Increased resolution of 1 nm with a reduced region of interest of 3.2 to 3.4 microns.

(d) De-noising using Wavelet Transforms

DWT De-noising is often an inbuilt function in many signal processing toolboxes and software modules. Here, we transform to the wavelet domain for finding DWT coefficients of each level (sub-band). After applying thresholding to estimated wavelet coefficients for each level, we reconstruct the de-noised signal by inverse DWT. However, such de-noising only works well with signals that have a smoother chemical spectrum (e.g. water as opposed to methane).

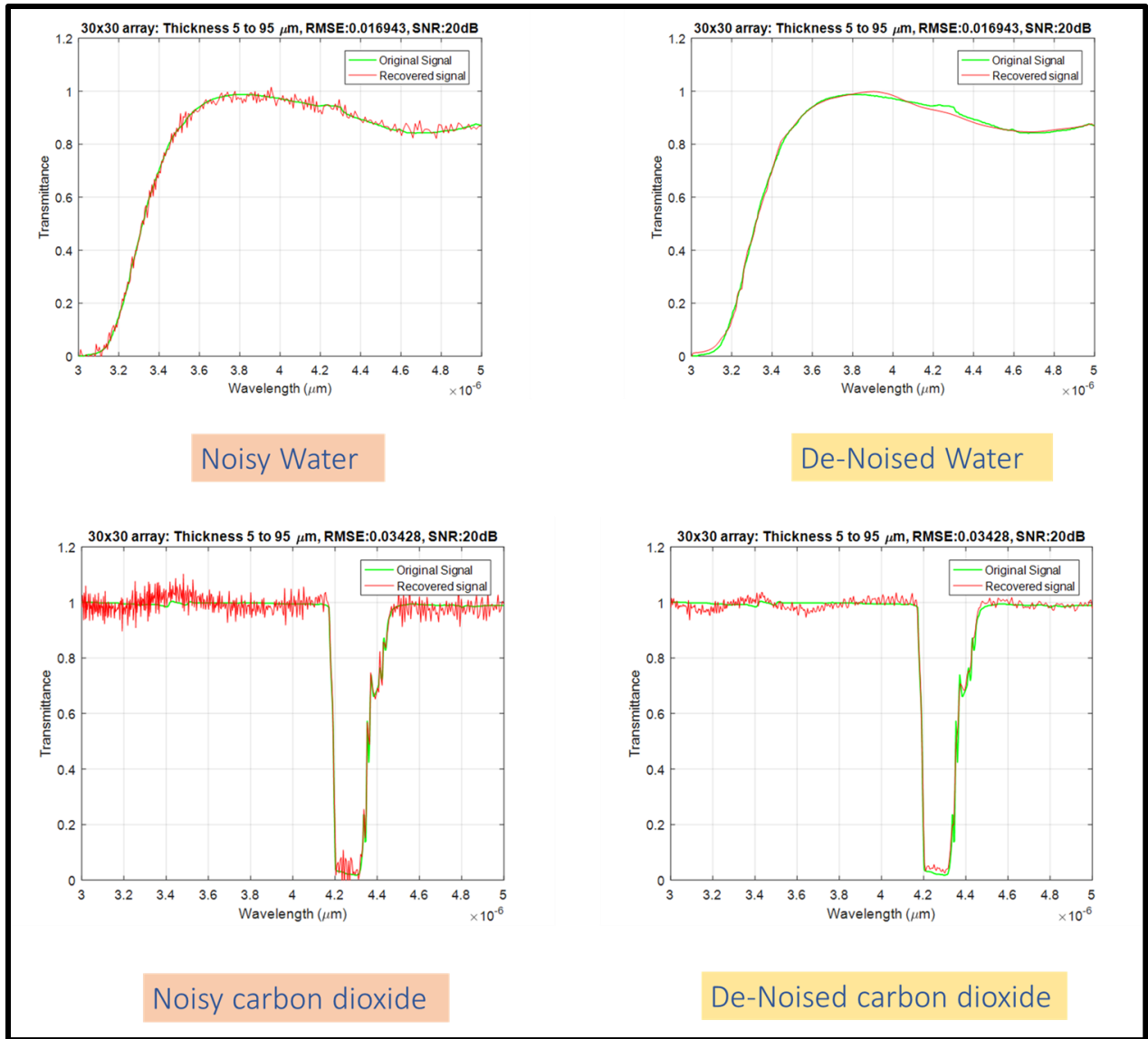


Figure 3.22: DWT De-noising

5. Opportunity

Examples in environmental monitoring and quality inspection.

Etalon arrays allow low-cost, compact and robust spectrometry with no moving parts.

Therefore, it is an excellent candidate for IR Spectrometers that is both inexpensive and small enough to integrate into handheld electronic devices. Once a device breaks this cost/size threshold, it then removes a critical barrier from the proliferation of the device. Much as the miniaturization and proliferation of inexpensive camera sensors have allowed their inclusion in everything from robots, laptop computers, and mobile phones, we expect that these small and cheap mid-IR spectrometers can be similarly integrated into a wide variety of systems. The ability to perform mid-IR spectroscopy in a portable form-factor, especially when combined with inexpensive thermal camera imaging, presents an exciting opportunity for IR spectroscopy. The 'Mid-Infrared' band roughly refers to electromagnetic radiation between 3 and 25 micrometers. Although there are many applications using light in this range, there are two in particular that make spectrometry and detection in this range useful. The first is that many molecular rotational and vibration signatures fall into this range, allowing mid-IR spectroscopy to detect and characterize the presence of specific molecules in a sample. The second is that black-body radiation from typical environmental temperatures fall into this

range, allowing for passive thermal vision and temperature measurements. As a result, mid-IR spectrometry has become an essential tool in science, medicine, and industry.

Following is a description of chemical sensing and identification with a change of basis scheme. Change of basis refers to a linear transformation scheme wherein we transform coordinate-wise representations of vectors taken with respect to one basis to their equivalent representations with another basis. Here, the linear projections of each chemical represented as a vector in wavelength space are taken onto the spectrum of the chemical to be identified (e.g. methane) in order to find correlations:

Change of Basis to Chemical Spectrum

Linear Transformation

$$[T]_{Chem\ Spectrum} = A_{\lambda \rightarrow Chem\ Spectrum} [T]_{\lambda}$$

$$[T]_{Chem\ Spectrum} = \begin{pmatrix} \overset{Chem_1}{\lambda_{11}} & \cdots & \overset{Chem_n}{\lambda_{n1}} \\ \vdots & \ddots & \vdots \\ \lambda_{1k} & \cdots & \lambda_{nk} \end{pmatrix} \begin{pmatrix} O_1 \\ \vdots \\ O_n \end{pmatrix}$$

Component Basis

$$\begin{pmatrix} O_1 \\ \vdots \\ O_n \end{pmatrix}$$

Where $A_{\lambda \rightarrow Methane}$ is simply a change of basis matrix representing the basis vectors of λ expressed in chemical spectra basis, consisting of $[T]$ vectors of the space in its columns:

For reconstruction:

$$Y = [A][T]_{Chem\ Spectrum}$$

Sensing Matrix:

$$[A][A_{\lambda \rightarrow Chem\ Spectrum}]$$

For n signals with k samples each, and for the representation of those samples in wavelength basis

Figure 3.23: Mathematical Representation of Spectrum Representation in a Sparse Basis. This basis is the chemical spectrum of interest.

Methane Leakage, Atmospheric Gases

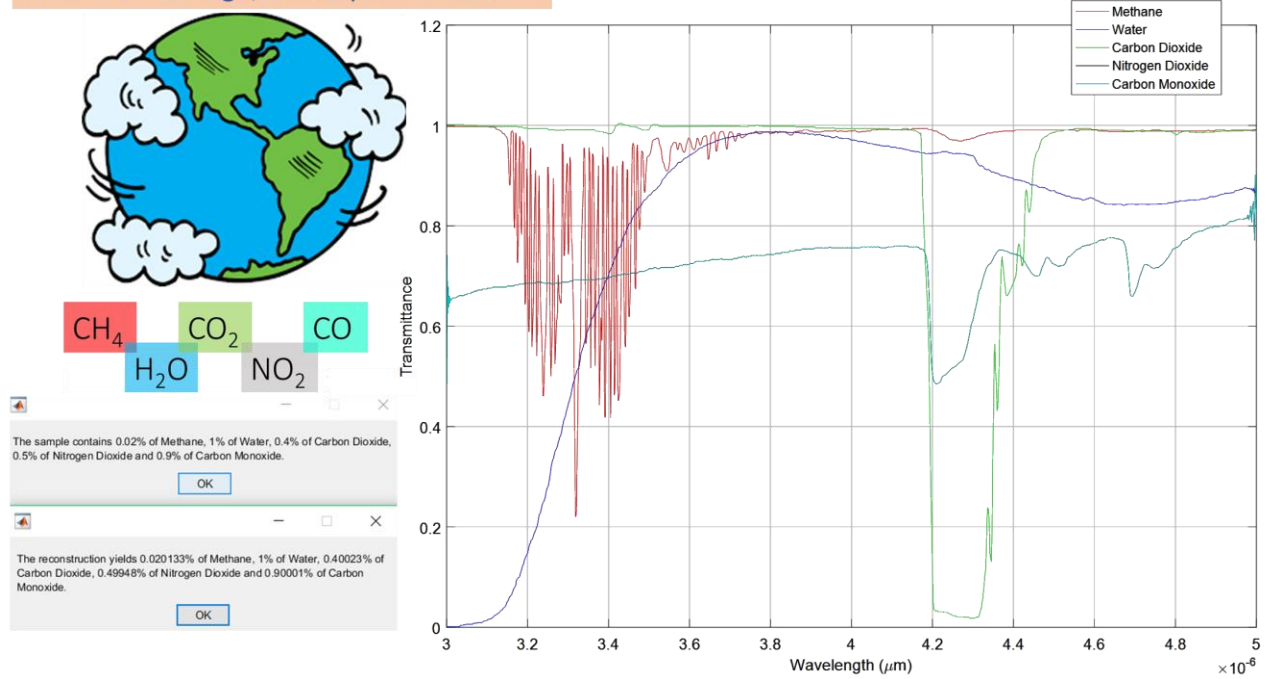


Figure 3.24: Accurate Identification of Chemical Sample in a Mixture. RMSE is as low as 0.00026% as there is only one point of measurement.

Tabulated Results per cavity array:

Table 3.2: Trends with increasing cavity array sizes. Increased number of cavities implies more resolution and reconstruction accuracy.

30x30 array presents the least RMSE values. The 10x10 array achieves a resolution of 20 nm before sparsity breaks! However, it could be useful for samples with known characteristic properties of the spectrum.

20x20 array

Starting Thickness	Maximum Thickness	Achieved Resolution	RMSE
200 nm	10 μm	20 nm	9.9355e-06
5 μm	10 μm	20 nm	0.0001437
5 μm	10 μm	14 nm	0.0063634
10 μm	50 μm	14 nm	2.8841e-05
10 μm	50 μm	6 nm	0.001344
30 μm	50 μm	6 nm	0.00232199
60 μm	100 μm	6 nm	0.0013703
5 μm	100 μm	2.5 nm	0.0266466

10x10 array

Starting Thickness	Maximum Thickness	Achieved Resolution	RMSE
100 nm	10 μm	25 nm	0.0017169
500 nm	10 μm	25 nm	0.0066819
1 μm	10 μm	25 nm	0.01086959
5 μm	10 μm	25 nm	0.003398
10 μm	50 μm	20 nm	0.001090685
30 μm	50 μm	20 nm	0.001561136
5 μm	100 μm	20 nm	0.0052235
60 μm	100 μm	20 nm	0.006069213

30x30 array

Starting Thickness	Maximum Thickness	Achieved Resolution	RMSE
5 μm	10 μm	20 nm	6.2106e-05
5 μm	50 μm	20 nm	2.2802e-06
5 μm	50 μm	4 nm	0.00059175
500 nm	50 μm	4 nm	6.9435e-05
10 μm	100 μm	4 nm	2.7948e-05
10 μm	100 μm	2.5 nm	0.00124792
30 μm	120 μm	2.5 nm	0.00039427

Table 3.3: CONCLUSION OF DESIGN ANALYSIS FOR EARS

Etalon Thickness	Larger optical thicknesses (~hundreds of μm) result in denser transmission spectra, with lesser separation between two successive transmission peaks.
	Greater resolution (level of detail) is attributed if the largest cavity is of this order (i.e. 10^{-4} m) for the MIR region. Also, reconstruction accuracy increases if thickness variation from the smallest cavity to the largest cavity is high.
	NOTE: Optical depth induces a higher attenuation coefficient and therefore should be commensurate in the chosen bandwidth of operation.
Etalon Array Size	Larger grids (e.g. 20x20 or 30x30) deploying greater number of cavities with different optical thicknesses give more measurements per capture.
	Higher reconstruction accuracy with increased information about the signal of interest. Since etalon array is directly overlaid on camera sensor, one-to-one pixel mapping possible.
	NOTE: In an attempt to match the pixel sizes on current image sensors, each etalon area could be very tiny causing diffraction effects if width is comparable with λ . Additionally, high SNR is required (>20 dB).
Etalon Mirror Design	Greater mirror reflectance (R) results in higher finesse which implies sharper transmission peaks.
	Reflective film of Al or Au with $R \sim 0.7$ in MIR gives better resolution as it governs the point spread function of the sampling pattern.
	NOTE: However, $R > 0.95$ degrades reconstruction accuracy. $R \sim 0.7$ provides a relatively broad peak which is needed to assimilate information across various wavelength points.
Material Considerations	Needed: substrate that is transparent to incident light in the wavelength of operation.
	Silicon (refractive index ~ 3.4 in MIR) is a suitable and inexpensive choice.
	NOTE: Material dispersion and thermal drift must be accounted, especially for larger bandwidth of operation.

References and Acknowledgements

1. P WT Yuen & M Richardson, *An introduction to hyperspectral imaging and its application for security, surveillance and target acquisition*, The Imaging Science Journal, 58:5, 241-253 (2010).
2. Atherton, P.D., N K. Reay, J. Ring, T. R. Hicks, *Tunable Fabry-Perot Filters*, Optical Engineering, 20, No.6, Pp. 806-814, (Nov/Dec. 1981).
3. Steinbruege, K.B., Gottlieb, M., and Feichtner, J.D. *Automatic Acousto-Optical Tunable Filter (AOTF) Infrared Analyzer*, Proc. SPIE 268, Imaging Spectroscopy, 1981.
4. V. Saptari, *Fourier-Transform Spectroscopy Instrumentation Engineering*, SPIE Press, Bellingham, WA (2003).
5. Noel H. Wan, Fan Meng, Tim Schröder, Ren-Jye Shiue, Edward H. Chen and Dirk Englund, *High resolution optical spectroscopy using multimode interference in a compact tapered fibre*, Nature Comm. 6, 7762 (2015).
6. Nahum Gat and Harold H. Szu, Martin Vetterli; William J. Campbell, James R. Buss, Ed, *Imaging Spectroscopy Using Tunable Filters: A Review*, Proc. SPIE Vol. 4056, p. 50-64, Wavelet Applications VII, (2001)
7. Horiba, *Jobin Yvon Spectrometer System: A six position filter wheel*.
8. J. Scheer, *Programmable tilting filter spectrometer for studying gravity waves in the upper atmosphere*, Applied Optics 26(15), pp. 3077–3082 (1987).
9. A. Stern, ed., *Optical Compressive Sensing* (CRC Press, 2016).
10. Eric Huang, Qian Ma and Zhaowei Liu, *Etalon Array Reconstructive Spectrometry*, Scientific Reports volume 7, Article number: 40693 (2017).

11. Yaniv Oiknine, Isaac August, Dan G. Blumberg, and Adrian Stern, *Compressive sensing resonator spectroscopy*, *Opt. Lett.* 42, 25-28 (2017).
 12. Junan Zhu and D. Baron, *Performance regions in compressed sensing from noisy measurements*, 47th Annual Conference on Information Sciences and Systems (CISS), Baltimore, MD, 2013, pp. 1-6 (2017)
-

Unconventional Hyperspectral Imaging

There's a spectrum in every pixel.

*"If a picture is worth a thousand words,
a hyperspectral image is worth almost thousand pictures"*

- *John Ferguson, MD (retd.),*

Photonics and Analytical Marketing Ltd.

1. Underlying Principle

Also known as imaging spectroscopy, hyperspectral imaging (HSI) is a technique to apply detailed spectral analysis on an imaged scene. It is a combination of a spectrometer stacked in front of a camera unit such that light reflected from an object is spectrally quantified before being imaged on a camera sensor array. Unlike regular imaging, which measures only three spectral bands (RGB), hyperspectral imaging acquires a series of contiguous bands and forms a data-cube with two dimensions containing the spatial image and one dimension storing

the spectral information¹. In other words, the scene is viewed under different continuous wavelengths such that each pixel contains a spectrum of its constituent matter. This analysis often extends beyond the visible spectrum into the infrared, which contains far more information about the molecular makeup of any substance, therefore making HSI very popular for target identification in remote sensing applications². It uncovers features invisible to the naked eye by traditional imaging. The imager was originally deployed for top-secret military surveillance in the 1980s. In the recent years, there has been resounding development in the field, with R&D efforts made to overcome the associated high costs and difficult data processing. With a boom in sophisticated computational methods^{3,4,5,6} for rapid data acquisition and processing, HSI is made almost ubiquitous in a variety of real applications like geographical mapping, environmental surveillance, weather forecasting, airport security, air and food quality inspection, archaeology and art conservation, medical diagnosis, surgical guidance, and many, many more. Additionally, with developments in fabrication techniques that produce small yet powerful sensors for imaging, compact hyperspectral imaging is now possible.

A typical hyperspectral imager samples light from a scene, in one of the four ways shown in figure 4.1, passes it through a slit, disperses it spectrally and focuses it onto the detector. For each pixel or raster cell position, the system plots a brightness value at each

wavelength to create a high-resolution spectrum for the image cell. The spectral resolution is determined by the spectrometer while the spatial resolution is determined by the imaging sensor.

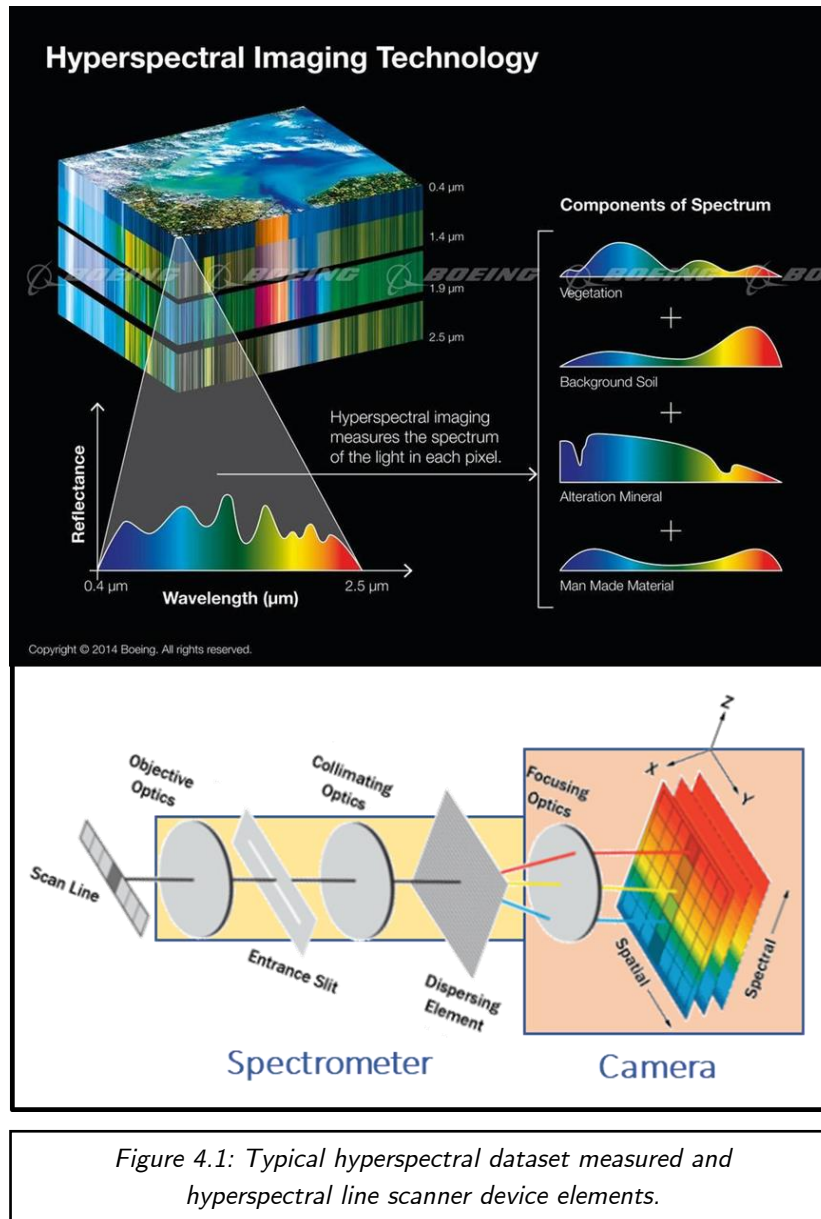
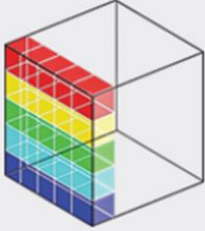


Figure 4.1: Typical hyperspectral dataset measured and hyperspectral line scanner device elements.

2. Hyperspectral datacube acquisition

HSI, despite its emerging applications and established need in almost every sector, is notorious for producing enormous datasets: each mega-pixel (i.e. one million pixels) picture is scanned through hundreds of data points per instantaneous field of view. Modern day processing chips are making it economically feasible, however we are still ways away from fast, high resolution spectral analysis per pixel. Our technique in compressive sensing offers a way to reduce the number of measurements made, thereby reducing processing complexity and still rendering high fidelity signals at video rates.

HSI sampling: Four techniques



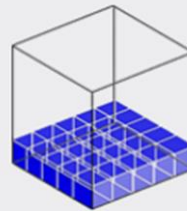
In **spatial scanning, or “pushbroom” imaging**, the system sweeps a slit aperture and grating across the spectral range in a single swath or line (x, λ) across a target area repeatedly over time, as the target passes in the y dimension (for example, on a conveyor belt application or from a satellite sweeping over an image area). The individual (x, λ) linescans are then combined in the y dimension into a hyperspectral data cube. A pushbroom system might also have a scanning mirror in front of the camera to capture the different lines of the target.



Snapshot or non-scanning imaging simultaneously captures both spectral and spatial information in a single image (x, y, λ) over a single integration time—using, for example, a large-format detector array capturing different wavelengths. No scanning is involved, so motion artifacts are eliminated and data processing simplified. That makes the technique ideal for low-resolution video rates, low-light imaging or high-speed applications.



Spatio-spectral scanning acquires a series of thin diagonal (x, y) slices of the data cube, each at every wavelength in the series. Typically, the system or camera must be scanned transverse to the slit. The dispersion-based system yields high spectral and spatial resolution, which is useful in astronomical imaging.



Spectral or “staring” scanning images a static or stationary scene in the (x, y) dimensions, while obtaining the λ dimension via the use of a tunable filter or stepping through a series of different pass-band filters over time. Spectral smearing can occur if the target area has movement, but it’s useful for applications like samples under a microscope.

Figure 4.2: Mechanisms to acquire the hyperspectral datacube⁷.

3. Contemporary Designs

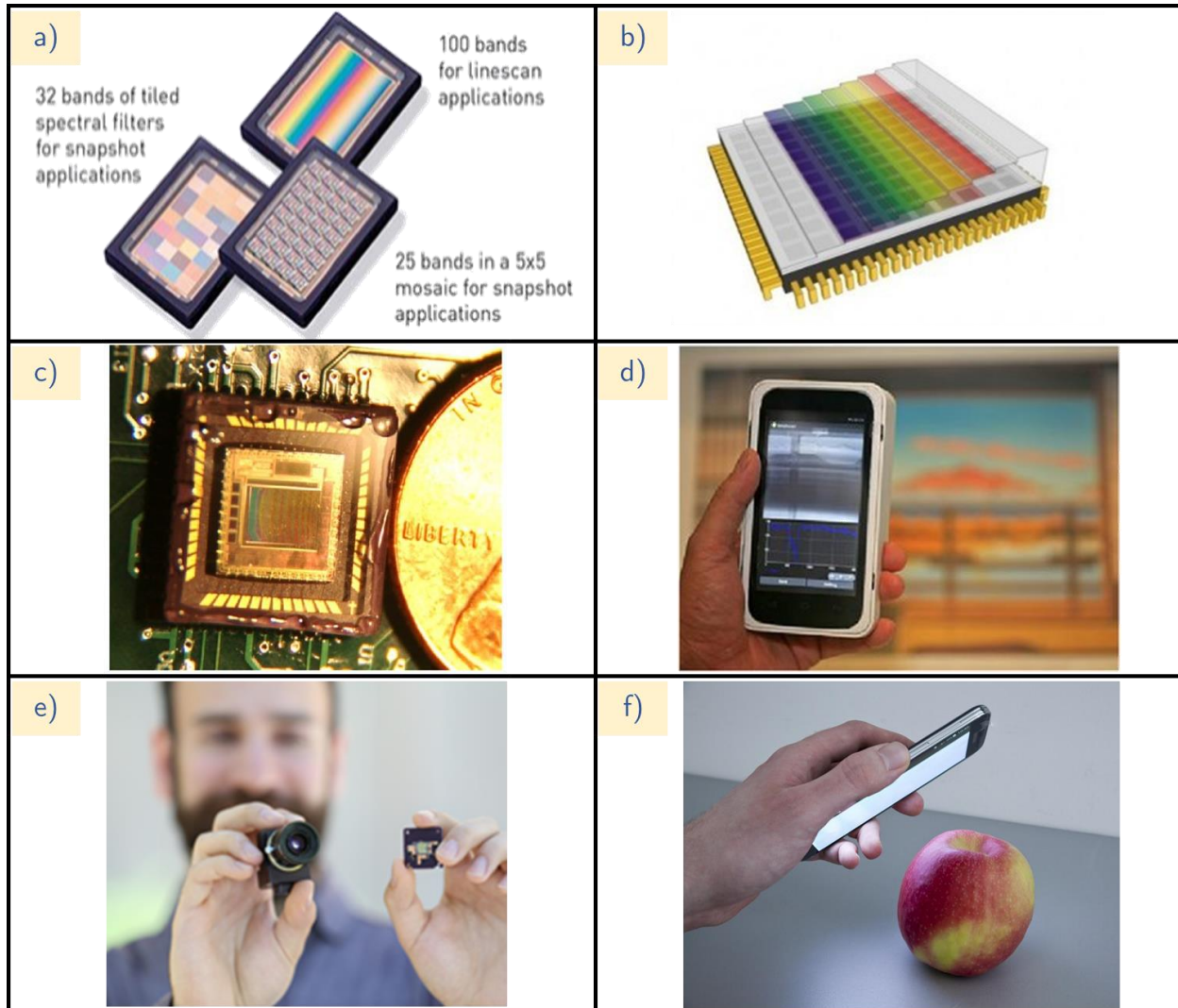


Figure 4.3: Recent Advancements in Compact Computational Hyperspectral Imaging

- a) IMEC broad range of integrated HS imagers based on CMOSIS CMV2000 image sensor⁸
- b) IMEC Multispectral Technology delineating filter fabrication with camera integration⁹
- c) Navy Research Lab MOSES based on FTIR; HS imager on UAV in conjunction with smartphone¹⁰
- d) BaySpec OCI™ HS snapshot handheld imager¹¹
- e) PARC Inc, Xerox; Polarization interferometer for Fourier imaging spectroscopy¹²
- f) Fraunhofer IFF HawSpex: brings HS imaging to Smartphones using an App¹³

4. Unconventional Hyperspectral Reconstruction using Spectral Resonance Modulation

Despite innovations in hyperspectral image rendering, many devices rely on continuous narrow band sensing while designing the spectrograph for measurement. While this technique has the capability of high resolution spectrum generation, the acquisition rate is often slower and/or compromises spatial resolution for spectral resolution. Additionally, such scanning routines using narrowband filters need to be very precise in filter design (e.g. for 4 nm resolution between 3 μm to 5 μm , we require ~ 500 precisely narrowband filters, where spectral response of each filter must span across 4 nm at FWHM). Our demonstrated technology consisting of a computational framework for spectrum reconstruction using compressive sensing proposes a way to enhance the performance of HS imagers to render real-time analysis at video rates, while also reducing the form factor for portable/hand-held ease of use.

For our purposes, a *complex datacube* is generated which consists of spatial information in (x,y) field of view of the camera but the spectral dimension (λ) is complex, just like in the case for EARS. This means, instead of adding tunable narrowband filters that scan across the wavelength region of interest, we use thickness variation through an etalon to scan across a snapshot of spectrally modulated (or encoded) signals that are demodulated (or decoded) post

detection using reconstructive algorithms. Here, each pixel is spatially calibrated for etalon transmission, forming a sensing matrix for each pixel. Depending on the sampling method, we introduce four methods for spectral resonance modulation by inducing the etalon thickness variation.

a. Piezoactuated Etalon Thickness Variation

This design is similar to the tunable Fabry Perot interferometer, where one mirror is held stationary while the other is translated relative to the first to control cavity thickness and thereby govern the interference pattern (transmission spectrum) generation. Cavity thickness is precisely tuned to allow a given narrowband wavelength range and block the rest. Our unconventional method uses the cavity thickness variation without such precise control requirements. The variation causes spectral modulation of the incident light, which acts as the sensing matrix for reconstruction post processing.

The setup for our unconventional hyperspectral imaging using compressive sensing is as follows: Two mirrors of desired R (reflectivity) on optically transparent substrates are held in kinematic mounts. One of them is fixed while the other is attached to a linear translation stage with piezoelectric

actuation in closed-loop configuration. The variation is achieved in defined steps depending on the resolution of the actuator. The cavity is placed in the infinity-corrected space of the camera front optics such that both the object and the cavity transmission are in focus.

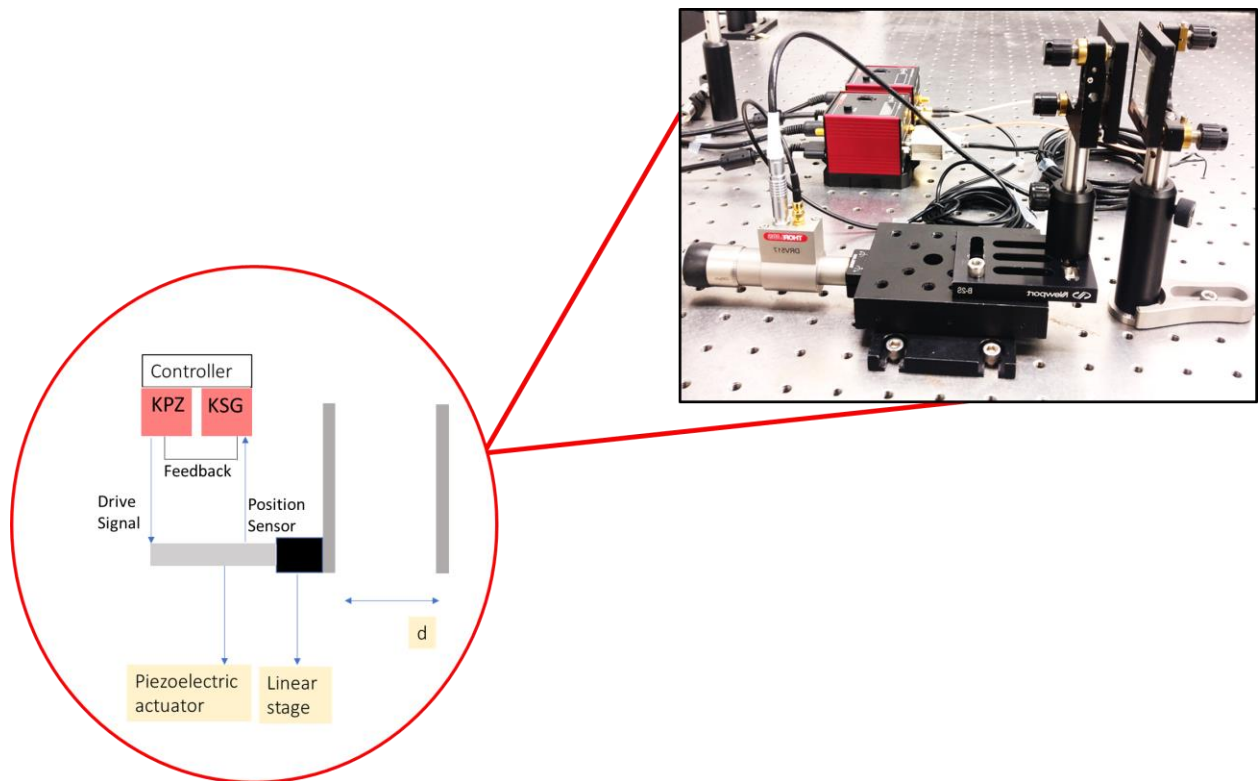


Figure 4.4: Closed-loop piezoelectric actuation for increasing mirror separation

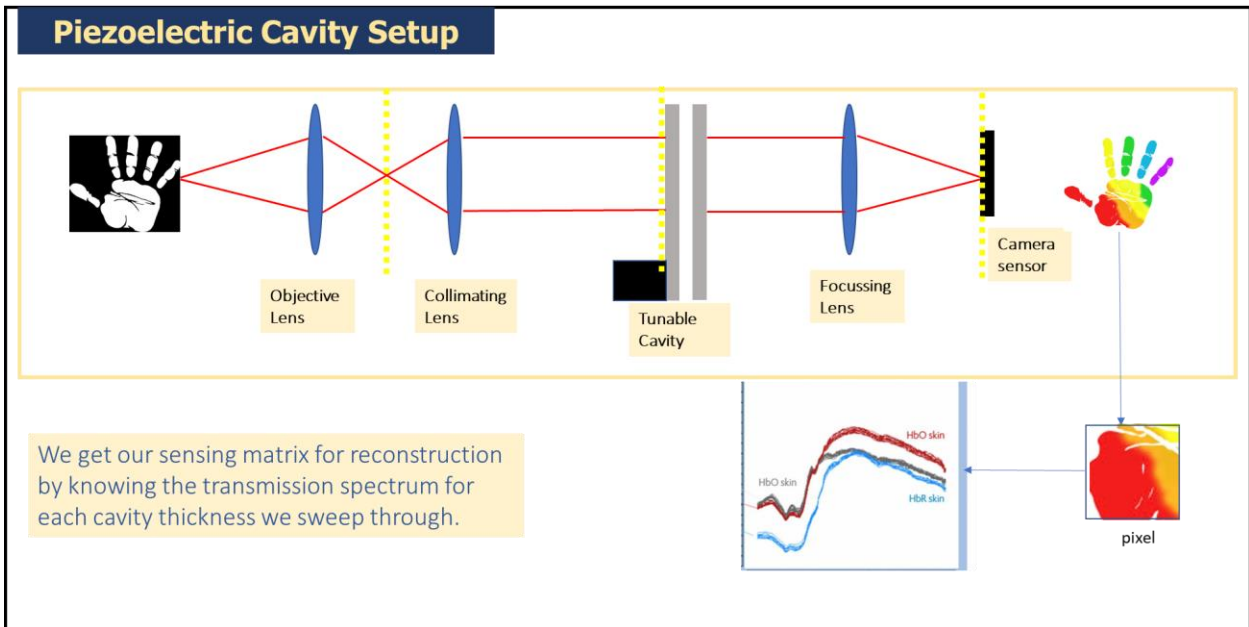
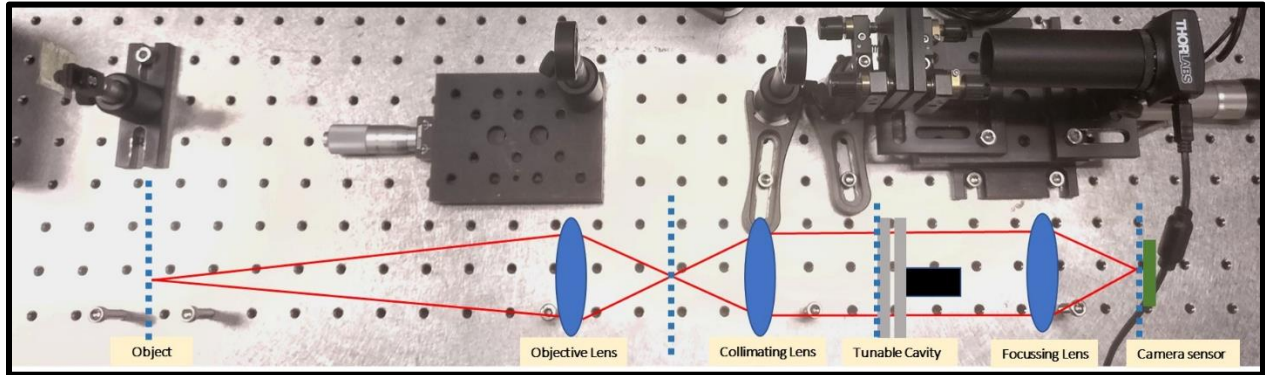
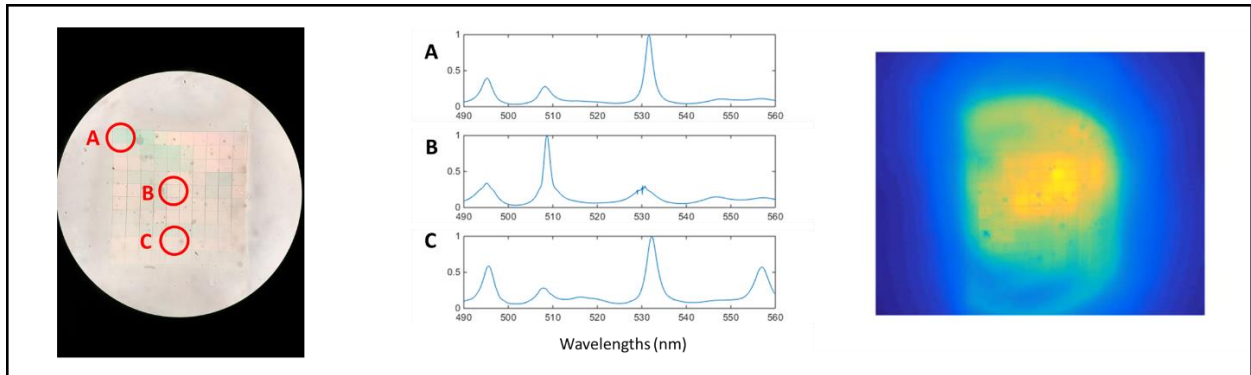


Figure 4.5: Schematic for optical setup for HSI with a tunable etalon

The piezoelectric actuated cavity gives more control over cavity thickness and thickness range for optimal reconstruction. The repeatability is also established, and the air gap is suitable for most operation ranges. As an example

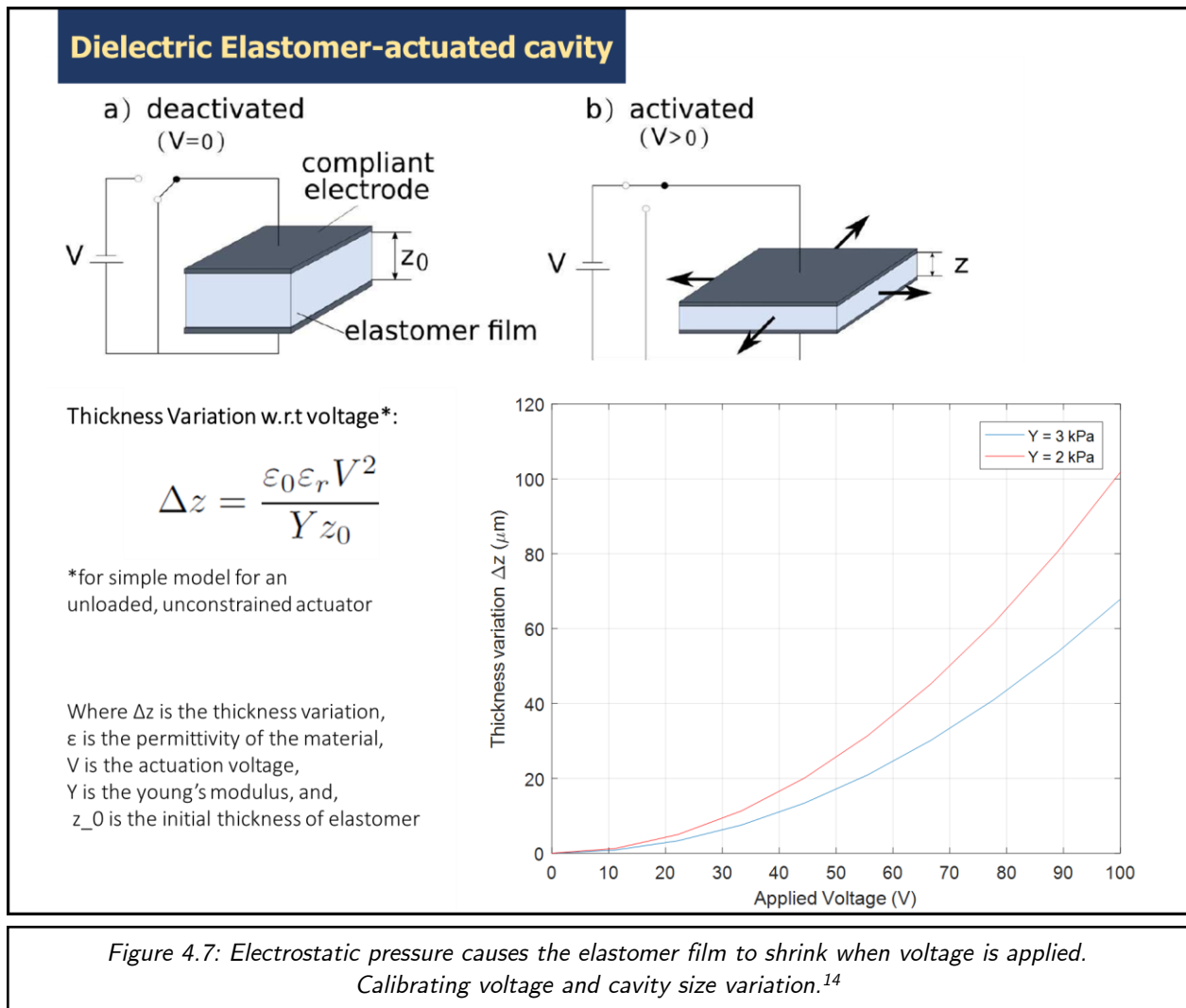
proof-of-concept, the cavity was used to characterize objects with sharp spectral features in the short wave infrared region, such as an etalon array cavity and a non-uniform film. The hyperspectral videos for both were reconstructed by sweeping across different cavity thicknesses. The calibration step requires that we fix the minimum distance of separation between the mirrors and back calculate the transmission spectrum to match this value. From here, we would increase the separation by controlled step sizes and use a monochromator for exact etalon transmission.



*Figure 4.6: Hyperspectral reconstruction with etalon array as test object.
A snapshot from the video is shown on the right.*

4.2 Elastomer-actuated Etalon Thickness Variation

Another method of varying cavity thickness is by method of using an elastomer as the spacer between the two mirrors forming an optical cavity, or etalon. When electricity is applied to such an elastomer, the elastomer shrinks and reduces in thickness due to electrostatic pressure. The relationship between voltage of actuation and thickness is given by:



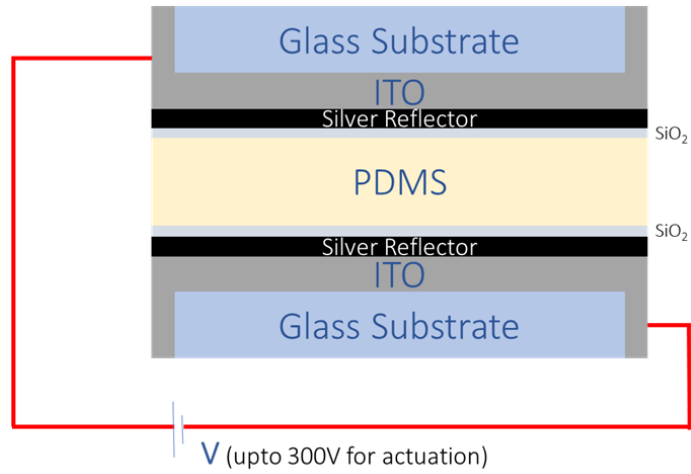


Figure 4.8: Etalon with elastomer spacer and electrical contacts for actuation.

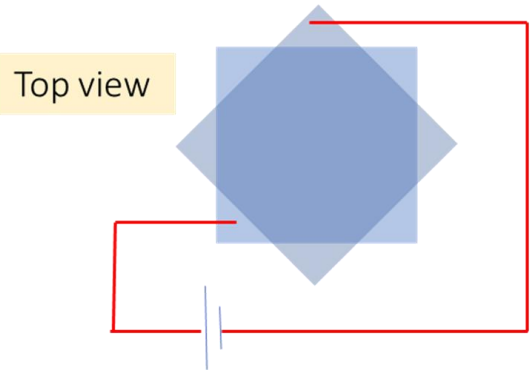
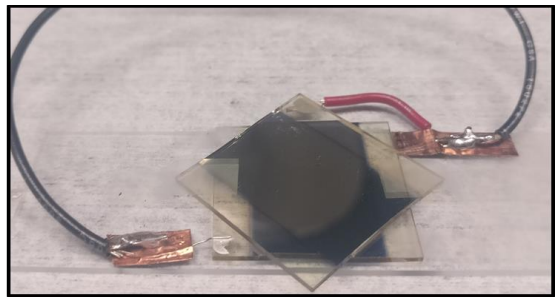


Figure 4.9: Establishing electrical contacts on the etalon.

The only challenge in this technique for etalon thickness variation is the very small change in thickness with very high actuation voltage step. This is also due to the added rigidity (young's modulus) in structure of the metallic mirrors. Rigid metallic films can have a stiffening effect on the PDMS spacer, especially if PDMS is not much thicker than the mirror thickness. Cracks can be formed due to less elasticity of metals during stretching of elastomer film. If instead, we have grooves or zig-zags on the surface of the metal, the rigidity would be greatly reduced, providing more thickness variation per voltage.

4.3 One Dimensional Stepped Etalon Array

Particularly useful for line scanner hyperspectral camera, a one-dimensional stepped etalon array ascribes a staircase structure only in one axis. Instead of a 10x10 or 20x20 or 30x30 arrays analyzed earlier in this study, the one-dimensional stepped etalon array is of the form 1x10 or 1x20 or 1x30. This creates a linear thickness variation only along one direction. Therefore, it measures a line of spatial information in one dimension and complex spectrum information in the other dimension simultaneously. It is like applying a complex sensing pattern to a line from the image, one line at a time. The data-cube is

then completed line-by-line by translating the array across the camera sensor and acquiring the image slices in multiple frames. Each pixel within a slice sees a different thickness of the etalon, and the sensing matrix is thereby generated. (Alternatively, a square array as discussed in section 3.2 could also be implemented, only with the same thickness variation across each row.)

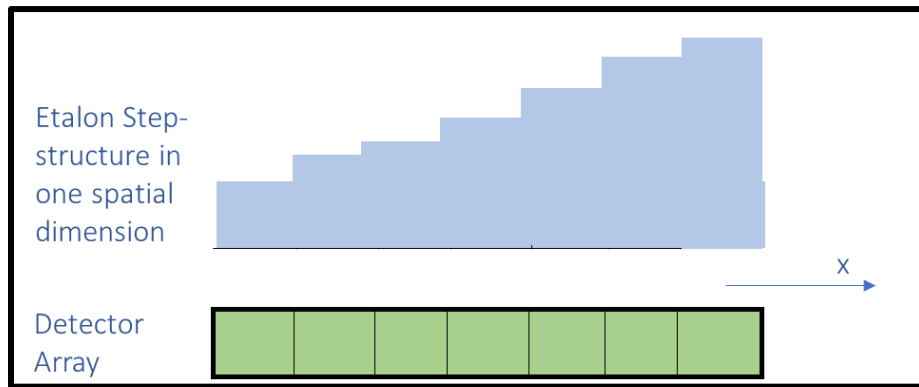


Figure 4.10 One Dimensional Stepped Etalon Array with variation only in one direction. Such an array be scanned through the object to encode each pixel of image line-by-line.

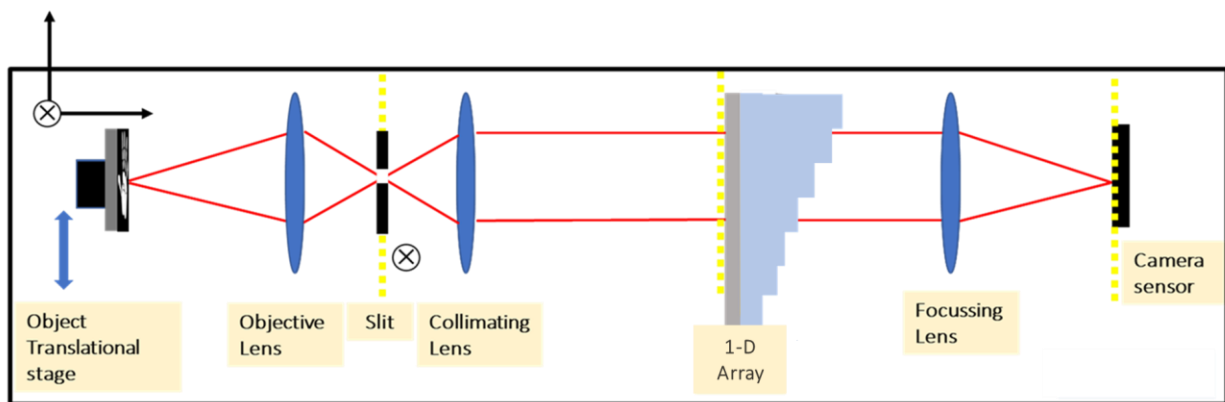


Figure 4.11: Schematic for optical setup for HSI with a one-dimensional etalon array

References and Acknowledgements

13. Honkavaara, T. Rosnell, R. Oliveira, A. Tommaselli, *Band registration of tuneable frame format hyperspectral UAV imagers in complex scenes*, ISPRS J. Photogramm. Remote Sens., 134 (2017), pp. 96-109
14. P WT Yuen & M Richardson, *An introduction to hyperspectral imaging and its application for security, surveillance and target acquisition*, The Imaging Science Journal, 58:5, 241-253 (2010).
15. T. Sun and K. Kelly, *Compressive Sensing Hyperspectral Imager*, in Frontiers in Optics 2009/Laser Science XXV/Fall 2009 OSA Optics & Photonics Technical Digest, OSA Technical Digest (CD) (Optical Society of America, 2009), paper CTuA5.
16. Jürgen Hahn, Christian Debes, Michael Leigsnering, Abdelhak M. Zoubir, *Compressive sensing and adaptive direct sampling in hyperspectral imaging*, Digital Signal Processing, Volume 26, Pages 113-126, ISSN 1051-2004 (2014).
17. A. Barducci, D. Guzzi, C. Lastrì, P. Marcoionni, V. Nardino, I. Pippi, *Compressive sensing and hyperspectral imaging*, Proc. SPIE 10564, International Conference on Space Optics — ICSO 2012, 105642Z (20 November 2017).
18. Gabriel Martín, José M. Bioucas-Dias, and Antonio Plaza, *HYCA: A New Technique for Hyperspectral Compressive Sensing*, IEEE Transactions on Geoscience and Remote Sensing, vol. 53, no. 5, (May 2015).
19. Chein I. Chang, *Hyperspectral imaging: techniques for spectral detection and classification*, (Plenum Pubs, 2003)
20. Pilar Gonzalez, Julien Pichette, Bart Vereecke, Bart Masschelein, Leonid Krasovitski, Leonid Bikov, Andy Lambrechts, *An extremely compact and high-speed line-scan hyperspectral imager covering the SWIR range*, Proc. SPIE 10656, Image Sensing Technologies: Materials, Devices, Systems, and Applications V, 106560L (14 May 2018)

21. Bert Geelen, Nicolaas Tack, Andy Lambrechts, *A compact snapshot multispectral imager with a monolithically integrated per-pixel filter mosaic*, Advanced Fabrication Technologies for Micro/Nano Optics and Photonics VII, Proc. of SPIE Vol. 8974 89740L-1
 22. Christopher C. Wilcox, Marcos Montes, Mike Yetzbacher, Jason Edelberg, Joseph Schlupf, *An ultra-compact hyperspectral imaging system for use with an unmanned aerial vehicle with smartphone-sensor technology*, Proc. SPIE 10639, Micro- and Nanotechnology Sensors, Systems, and Applications X, 1063919 (8 May 2018).
 23. Huawen Wu, Frederick G. Haibach, Eric Bergles, Jack Qian, Charlie Zhang, William Yang, *Miniaturized handheld hyperspectral imager*, Proc. SPIE 9101, Next-Generation Spectroscopic Technologies VII, 91010W (21 May 2014).
 24. Alex Hegyi and Joerg Martini, *Hyperspectral imaging with a liquid crystal polarization interferometer*, Opt. Express 23, 28742-28754 (2015).
 25. Michael Schenk, Udo Seiffert and Hans-Christian Klück, *Hawkspex®: A Flexibly Configurable Hyperspectral Camera*, Fraunhofer Institute for Factory Operation And Automation IFF (2012)
 26. Irma Slowik, Nils M. Kronenberg, Markus Franke, Axel Fischer, Andreas Richter, Malte C. Gather and Karl Leo, *Elastomer based electrically tunable, optical microcavities*, Appl. Phys. Lett. 109, 171104 (2016).
-

Epilogue

EARS is a computational, complex, camera-based spectrometric method that yields ultracompact, inexpensive, robust, fixed spectrometer design with broadband, high-resolution, fast spectral acquisition capability.

The objective of this thesis was to identify and implement the design parameters of the etalon array for unconventional reconstructive spectrometry, thus finding a reasonable fit for the hardware and software framework that resulted in least root mean squared error (RMSE) post processing. An additional purpose of the study was to develop an optical resonator mechanism for a hyperspectral imager such that a similar reconstruction regime could be applied for compact, high-performance and high-resolution hyperspectral image rendering.

“Be curious, I know I will forever be.”

- Stephen Hawking

Patent Disclosure for Reconstructive Hyperspectral Imager using Tunable Fabry Perot Cavity
UCSD Docket No. SD2018-106

Collaboration and funding acknowledgement: DRS Technologies and Moore Foundation.